

POLITECNICO DI TORINO
Master's Degree in Biomedical Engineering



**Politecnico
di Torino**

Master's Degree Thesis

**Computational investigations of the link
between hyperphosphorylation of MAP tau
and melatonin binding in Alzheimer's disease**

Supervisors

Prof. Jack TUSZYNSKI

Prof. Marco DERIU

Candidate

Luca CONGIU

MARCH 2023

Acknowledgements

Contents

Acronyms	viii
1 Biological Background	1
1.1 Alzheimer's Disease	1
1.2 Tau protein	2
1.3 Kinases and Phosphatases	4
1.3.1 Kinases and Phosphatases as drug targets	7
1.4 Temperature and Alzheimer's disease	8
2 Computational Methods	11
2.1 Structures	11
2.2 Molecular Operating Environment	12
2.2.1 Homology modelling	12
2.3 Molecular modelling	12
2.4 Molecular Mechanics	13
2.4.1 Potential Energy Function	13
2.4.2 Periodic Boundary Conditions	15
2.4.3 Potential Energy minimization	16
2.5 Molecular Dynamics	17
2.5.1 Statistical ensemble	17
2.5.2 Molecular Dynamics implementation scheme	19
2.6 Binding free energy prediction	20
2.7 Molecular Docking	21
2.7.1 Consensus docking	21
2.8 Electrostatic profile	22
3 Results and discussion	24
3.1 Electrostatic maps	24
3.2 Molecular Dockings	30

3.3	Molecular Dynamics results	40
3.4	Free-binding energy estimation	48
4	Conclusions	60

List of Tables

3.1	PLB values, Not-Human structure. Bold values indicate binding sites that do not overlap with the GTP/GDP binding site.	31
3.2	PLB values, Human structure. Bold values indicate binding sites that do not overlap with the GTP/GDP binding site.	31
3.3	Docking results, dimer1 non-human	32
3.4	Docking results, dimer2 non-human	32
3.5	Docking results, dimer3 non-human	33
3.6	Docking results, dimer4 non-human	33
3.7	Docking results, dimer5 non-human	34
3.8	Docking results, dimer6 non-human	34
3.9	Docking results, dimer7 non-human	35
3.10	Docking results, dimer1 Human structure	35
3.11	Docking results, dimer2 Human structure	36
3.12	Docking results, dimer3 Human structure	36
3.13	Docking results, dimer4 Human structure	37
3.14	Docking results, dimer5 Human structure	37
3.15	Docking results, dimer6 Human structure	38
3.16	Docking results, dimer7 Human structure	38
3.17	Free-binding energy of the melatonin-dimer binding [kJ/mol, Non-human structure]	38
3.18	Free-binding energy of the melatonin-dimer binding [kJ/mol], human structure	39
3.19	Free-binding energy [kJ/mol], Tau-Microtubules, No-melatonin	48
3.20	Free-binding energy [kJ/mol], Tau-Microtubules with melatonin	48
3.21	Free-binding energy [kJ/mol], Tau-Microtubules with melatonin	49
3.22	Free-binding energy [kJ/mol], Tau-Microtubules, No-melatonin	50

List of Figures

1.1	a) The Human MAPT gene encodes six tau isoforms that are resulted from alternative splicing of exons 2, 3, and 10. N1 and N2 are the N-terminal inserts. P1 and P2 are the two proline-rich regions. R1 to R4 are the four microtubule-binding repeats. R is the C-terminal repeat-like region. b) Amino acid sequence of 2N4R tau isoform. [1]	4
2.1	Two-dimensional representation of periodic boundary condition.	16
2.2	Representation of the Potential Energy surface.	17
2.3	Simplified scheme of a Molecular Dynamics algorithm	20
2.4	Flowchart demonstrating the sequence of operations performed by the pipeline. The process begins with an input PDB file and ends with a parameterized PQR file and, optionally, an APBS input file.[2]	23
3.1	Electrostatic map of the structure, front view	24
3.2	Electrostatic map of the structure, side view	25
3.3	Electrostatic map of SER202, SER208, SER210, SER214	25
3.4	Electrostatic map of SER235, SER237, SER238, SER241	26
3.5	Electrostatic map of SER258, SER262	27
3.6	Electrostatic map of SER285, SER289, SER293	28
3.7	Electrostatic map of SER305	28
3.8	Electrostatic map of SER316, SER320, SER324	29
3.9	Electrostatic map of SER341, SER352, SER356	29
3.10	Detail of the structure with the melatonin inserted	40
3.11	Minimization results, structures without melatonin	41
3.12	Minimization results, structures with melatonin	42
3.13	NVT equilibration, structures without melatonin	43
3.14	NVT equilibration, structures with melatonin	43
3.15	RMSD values, 11 simulations of 100ns, 7pqc	44
3.16	RMSD values, 11 simulations of 100ns, 7pqc human	44
3.17	RMSD values, 11 simulations of 100ns, 7pqc phosphorylated	45

3.18	RMSD values, 11 simulations of 100ns, 7pqc human - phosphorylated	45
3.19	RMSD values, 11 simulations of 100ns, 7pqc with melatonin	46
3.20	RMSD values, 11 simulations of 100ns, 7pqc human with melatonin	46
3.21	RMSD values, 11 simulations of 100ns, 7pqc phosphorylated with melatonin	47
3.22	RMSD values, 11 simulations of 100ns, 7pqc human- phosphorylated with melatonin	47
3.23	Free-binding energy of the binding of serines to microtubules. 7pqc	51
3.24	Free-binding energy of the binding of serines to microtubules. Hu- man 7pqc	52
3.25	Free-binding energy of the binding of serines to microtubules. Phos- phorylated 7pqc	53
3.26	Free-binding energy of the binding of serines to microtubules. Human-phosphorylated 7pqc	54
3.27	Free-binding energy of the binding of serines to microtubules. 7pqc with melatonin.	55
3.28	Free-binding energy of the binding of serines to microtubules. Hu- man 7pqc with melatonin.	56
3.29	Free-binding energy of the binding of serines to microtubules. Phos- phorylated 7pqc with melatonin.	57
3.30	Free-binding energy of the binding of serines to microtubules. Human-phosphorylated 7pqc with melatonin.	58

Acronyms

A β β -Amyloid 1, 2, 8

AD Alzheimer's Disease ix, 1, 2, 4–8

APP Amyloid Precursor Protein 2

CaMKII calcium/calmodulin-dependent protein kinase II 6, 7

CK1 Casein Kinase-1 6

CTD C-terminal domain 3

GSK3 glycogen synthase kinase-3 5–9

HD Huntington's disease 2

MTBD microtubule-binding domain 3

NFTs Neurofibrillary tangles 1, 2

NTD N-terminal domain 3

PD Parkinson's disease 2

PDPKs proline-directed protein kinases 5, 7

PHFs paired helical filaments 2, 5

PiD Pick's disease 2

PRD proline-rich domain 3

Abstract

Alzheimer's Disease (AD) is one of the most impacting neurodegenerative diseases worldwide. The current work aims to deep into one of the principal hypotheses investigated in the research to find an effective cure for *AD*: the Tau hypothesis. According to the Tau hypothesis, Alzheimer's disease is derived primarily from the hyperphosphorylation of protein MAP Tau, which makes it detach from microtubules, leading to their disruption and so to neuronal death. More in-depth, current research is focusing on the role of temperature and melatonin on the modulation of Tau hyperphosphorylation. Temperature appears as a determining modulator of the activity of kinases and phosphatases, apparently through the modulation of the body's melatonin production and distribution. Computational tools allowed us to perform atomic simulations and free-binding energy calculations of a system representative of a microtubule protofilament stabilized by the Tau protein's microtubule-binding domain, both with and without the phosphorylation of Tau serines. In addition, the role of melatonin in modulating this bind has been investigated. In this way, it has been possible to collect energy data on the system in Alzheimer-like conditions.

1

Biological Background

1.1 Alzheimer's Disease

The **AD** is a neurodegenerative disease first described by Aloise Alzheimer in 1908. Among the neurodegenerative diseases, it is the one with the major impact at the global level, with an estimated population of 6.5 million affected by this disease only in the US and 50 million worldwide[3]. AD is a form of dementia, and so it manifests with a progressive cognitive deficit that starts with a memory decline and proceeds with an impairment of visual-spatial skills, language and executive functions. The major risk factor is ageing but currently, also others have been identified such as genetic factors, smoking, traumatic brain injuries, depression and metabolic factors such as diabetes mellitus, obesity and low HDL cholesterol[4]. Anyway, the main mechanism that led to the development of AD remains obscure and, consequently, the possibility to design an effective therapeutic strategy.

The main hallmarks of AD are the presence of **Neurofibrillary tangles (NFTs)** into the neuron body[5] and β -amyloid plaques in the brain's extracellular environment[6] that, combined, cause brain atrophy. These two findings gave rise to the two principal hypotheses that during the last decades tried to explain the pathological evolution of the **AD**: the Tau hypothesis and the Amyloid cascade hypothesis.

Amyloid plaques are extracellular insoluble deposits of **β -Amyloid ($A\beta$)**. The

$A\beta$ is formed by the cleavage of a trans-membrane protein called **Amyloid Precursor Protein (APP)** by the α , β and γ -secretases. In particular, the APP cleaved by the γ -secretases followed by the cleavage of the α -secretases produced a 40-aminoacids peptide called $A\beta_{40}$. If the action of the α -secretases is substituted by the β -secretase there is the production of a longer amyloid fragment called $A\beta_{42}$ that is considered the most neurotoxic amyloid species according to the Amyloid cascade hypothesis. The $A\beta_{42}$ has a high tendency to aggregate forming firstly small oligomers that act as primary nucleation sites for the formation of the fibrils. Interestingly, most of the oligomers resulted from the fibrils themselves through a secondary-nucleation mechanism and so, the fibrils are generated by a positive-feedback loop[7]. However, it is worth noting that recently the Amyloid-hypothesis was questioned after the discovery of data falsification in the main works on which the hypothesis was based[8].

On the contrary, according to the Tau hypothesis, neurodegeneration in **AD** is due to abnormal phosphorylation of the protein MAP-tau that causes it to detach from microtubules and, consequently led to their disruption. The detachment of Tau protein is followed by its aggregation firstly in **paired helical filaments (PHFs)** and then in **NFTs**. The presence of **NFTs** is a main feature observed in many neurodegenerative diseases including **Parkinson's disease (PD)**, **Huntington's disease (HD)** and **Pick's disease (PiD)** that are now known as tauopathies. Regarding the **AD**, this hypothesis was first developed in 1986, when it was established that the constituent of the **NFTs** was the protein MAP-tau[5]. In the same year, other breakthrough discoveries were made: Binder *et al.* highlighted the presence of abnormal levels of hyperphosphorylated Tau in **AD**[9] and Ogawara *et al.* proved that the hyperphosphorylated tau was the major constituent of the **NFTs**[10]. The Tau hyperphosphorylation seems to be a consequence of the dysregulation of the enzymes kinase and phosphatase. One of the main pieces of evidence that support this hypothesis is that the levels of protein Tau in the brain directly correlate to the severity of the disease. Such correlation is not observed for the $A\beta$. Currently, there is no agreement on what causes the hyperphosphorylation of tau and there is also no proof of whether the hyperphosphorylation is a cause of the detachment or a consequence.

1.2 Tau protein

Tau protein is a microtubule-associated protein first discovered in 1975[11]. It is encoded by the MAPT gene, which is located on human chromosome 17. Six tau

isoforms (0N3R, 0N4R, 1N3R, 1N4R, 2N3R, 2N4R) are generated by alternative splicing of exons 2, 3 and 10[12, 13]. The tau isoforms differ by having zero (0N), one (1N) or two amino-terminal (2N) insert and three (3R) or four (4R) microtubule-binding repeat sequences. Tau can be found in the central and peripheral nervous systems and, in particular, in the axons, where its main function consists of promoting microtubule assembly and stabilization. Tau is highly soluble but can aggregate into insoluble fibers. Tau protein is an intrinsically disordered protein and so techniques such as nuclear magnetic resonance and small-angle x-ray scattering failed to discern a precise three-dimensional structure[14]. However, the nuclear magnetic resonance, circular dichroism and Fourier transform infrared spectroscopy highlighted the presence of transient secondary structures[15, 16]. Tau protein structure is characterized by four different regions: the **N-terminal domain (NTD)**, the **proline-rich domain (PRD)**, the **microtubule-binding domain (MTBD)** and the **C-terminal domain (CTD)**. The **MTBD** is mainly negatively charged and it presents three or four microtubule-binding repeat sequences, depending on the iso-type. 3R isotypes missed R2 binding sequence. **MTBD** presents two aggregation-prone hexapeptide motifs, PHF6* (²⁷⁵VQIINK²⁸⁰) and PHF6 (³⁰⁶VQIVYK³¹¹), respectively located on R2 and R3 binding repeats. These two hexapeptides adopt β -strand conformations[17] and are essential for the aggregation of Tau. The N-terminal domain

1.3. KINASES AND PHOSPHATASES

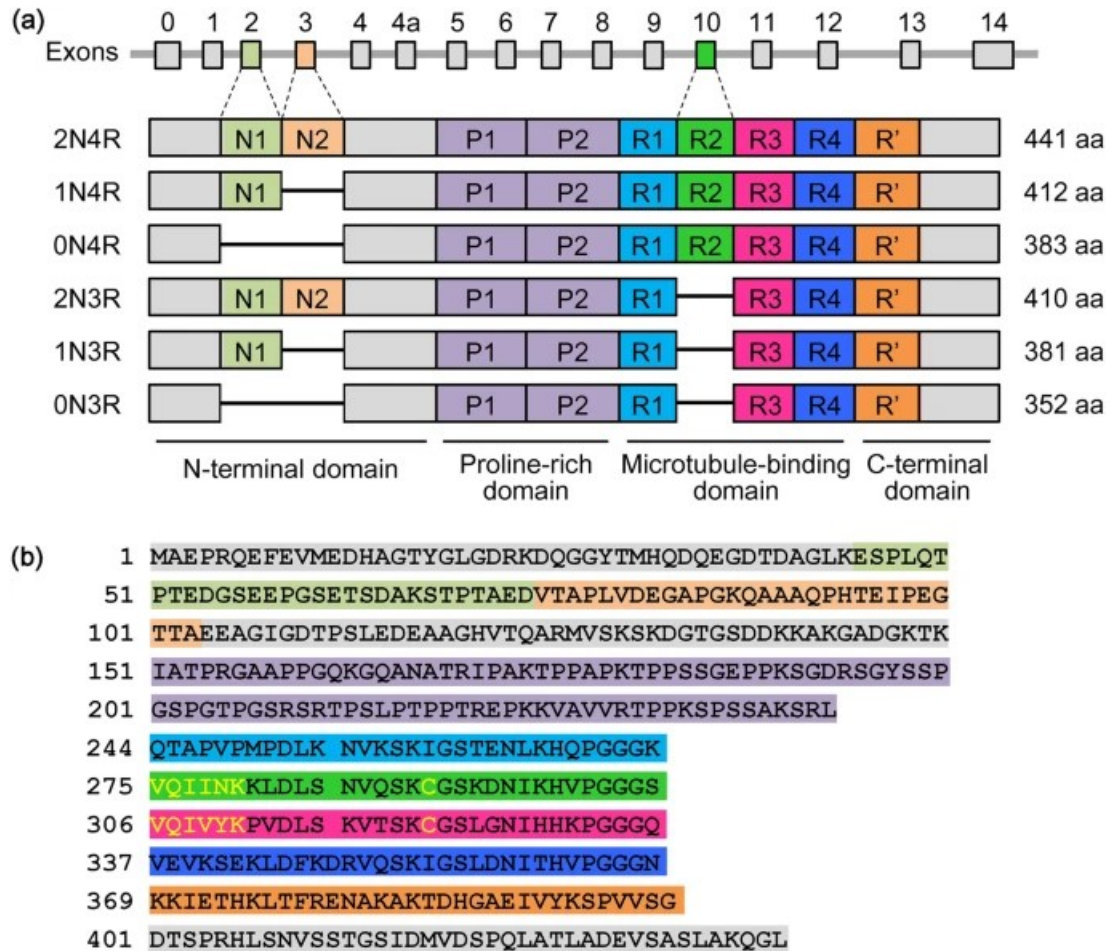


Figure 1.1: a) The Human MAPT gene encodes six tau isoforms that are resulted from alternative splicing of exons 2, 3, and 10. N1 and N2 are the N-terminal inserts. P1 and P2 are the two proline-rich regions. R1 to R4 are the four microtubule-binding repeats. R is the C-terminal repeat-like region. b) Amino acid sequence of 2N4R tau isoform. [1]

1.3 Kinases and Phosphatases

As said below, Tau Hypothesis assumes that the main neurodegeneration driver in Alzheimer's Disease is the hyperphosphorylation of MAPtau. In 1993, Iqbal *et al.* firstly estimate the levels of phosphorylation of Tau in AD patients' brains [18]. According to their work, Tau is found 3-4 fold more phosphorylated in AD brains than in control brains. In particular, it is reported a concentration of 8 PO₄/mol for

pathological tau. Follow-up studies showed that pathological tau found in PHFs has at least 40 phosphate groups out of 80 sites found in the 441-tau isoform. In addition, today several Tau phosphorylation sites and the respective kinases are well known: [//www.kcl.ac.uk/people/diane-hanger](http://www.kcl.ac.uk/people/diane-hanger).

Following these works, more studies were conducted to elucidate which kinases and phosphatases were involved in the mechanism of Tau phosphorylation. Taking into account the high amount of phosphorylated residues, all the studies converge to attribute these results to the synergistic activity of more than one kinases[19, 20, 21]. Kinases are enzymes that catalyze the transfer of phosphate groups from high-energy molecules to specific substrates. On the contrary, phosphatase enzymes catalyze the hydrolysis of the phosphoester bound between the phosphate group and the respective residue. Currently, several **proline-directed protein kinases (PDPKs)** and non-PDPKs have been identified. Among the PDPKs we include MAP kinase, cdc-2 kinase, cdk-2, cdk-5 and GSK-3. Non-PDPKs include PKA, C-kinase, CaMKII, CK-1 and CK-2.

Anyway, the kinases mostly involved in the tau hyperphosphorylation are considered from **glycogen synthase kinase-3 (GSK3)** family. GSK3 were discovered as inhibitors of glycogen synthase and have rapidly been associated with several other physiological and pathological functions. Currently, two GSK3 isoforms has been found, respectively named GSK3 α and GSK3 β . These two isoforms share an 80% of similarity and the former is the most studied of the two. Expression levels of this enzyme family were found to increase in AD brains, although its activation was unchanged[22]. Among the 80 phosphorylation sites found in Tau, GSK3 β phosphorylates at least 30 of them, depending on the phosphorylation state of Tau[20, 19, 23]. One of the first studies that linked the activity of GSK3 with hyperphosphorylated Tau was conducted by Mendelkowitz et al. in 1992 which tested several kinases of the PDPKs family[19]. Following this work, several other studies tried to characterise the residues phosphorylated by GSK3, alone and in combination with other kinases. The main concept carried on during the following years was that, assuming the central role of GSK3 in the Tau hyperphosphorylation, it is necessary cooperation between PDPKs and non-PDPKs to obtain a pathological level of phosphorylation. Iqbal *et al.* in 1995 demonstrated this phenomenon for the first time[24]. In particular, they investigated how the capability of GSK3 to phosphorylate Tau changes after a pre-phosphorylation of different non-PDPKs. They found out that a pre-phosphorylation by PKA, PKC or CK-2 augmented the subsequent phosphorylation by GSK3. On the contrary, pre-phosphorylation by CK-1, CaMKII or Gr kinase did not enhance subsequent GSK3 phosphorylation. In 1998 they deepened this study by evaluating GSK3 activity with PKA or CK-1

and trying to find out which phosphorylation sites are phosphorylated with different combinations of kinases. They discovered that the pre-phosphorylation by PKA was the one that strengthened the subsequent phosphorylation of GSK3[20]. In particular, GSK3 alone was capable to phosphorylate Ser-181, Ser-184, Ser-262 and Ser-400 whether, in combination with PKA, phosphorylates Ser-195, Ser-198, Ser-199, Ser-202, Thr-205, Thr-231, Ser-235 and Ser-262. In 2007, they proposed again a similar work which focused on different combinations of GSK3, CaMKII, PKA and cdk5 as well as on the role of PP2A (which will be discussed later)[21]. Anyway, they showed that kinases alone failed to completely rephosphorylate the Tau after dephosphorylation by PP2A. In particular, the only combination of kinases able to completely cover the PP2A work was PKA, CaMKII and GSK3 β by phosphorylating Ser-198, Ser-199, Ser-202, Thr212, Ser-214, Ser-262, Ser356, Ser396, Ser404, Thr181, Ser199, Ser202, Thr212, Ser214, Ser217, Thr231, Thr403. However, the majority of the phosphorylation sites overlap with the GSK3 β activity alone. So, these studies proved the central role of GSK3 β in the development of pathological hyperphosphorylated Tau but they showed also that, for the arising of a pathological state it is necessary the synergic work of more than one kinase. Finally, Rankin *et al.* demonstrated that GSK3 is sufficient to initiate a Tau aggregation similar to the one seen in AD. Anyway, it is worth noting that arachidonic acid was used to help the aggregation[25].

Casein Kinase-1 (CK1) is another kinase strongly associated with neurodegeneration. Currently, six isoforms (α , β , δ , γ 1-3 and ϵ) have been characterised[26, 27]. Studies about the spatial distribution of these isoforms asserted that CK1 α and CK1 δ are the ones mainly found in AD brains, where the former has been mainly associated with Neurofibrillary tangles and the latter with granulovacuolar degeneration bodies. Anyway, among the two, CK1 δ concentration in AD brains is found elevated 30-fold and its distribution directly correlates with the spreading of the pathology[28]. Moreover, CK1 δ phosphorylates almost all the Tau sites found in AD and, in particular, it phosphorylates the sites that participate in tau-microtubule binding[29]. In particular, GSK3 and CK1 together account for almost all the Tau-kinase activity[30]. For this reason, CK1 became, along with GSK3, one of the main pharmacological targets for the treatment of AD.

Another kinase strongly associated with AD is the calcium/calmodulin-dependent protein kinase II (CaMKII). CaMKII is a large holoenzyme composed of a six-domains central hub linked to twelve kinase domains[31]. Its activity is thought to be essential for memory encoding and long-term potentiation[32, 33]. Regarding AD, CaMKII is able to phosphorylate the main tau residues involved in the tau-microtubule binding. In particular, it is the main kinase the phosphorylate

Ser-262 and Ser-356. Phosphorylation of these two residues accounts for almost 40% of the tau-microtubule energy binding. In 1993, it was first shown that phosphorylation of Ser-262 was necessary but non sufficient to completely detach tau from microtubules[34]. Starting from that work, it was at the end demonstrated that **CaMKII** was the main enzyme, among all the non-PDPKs responsible for the phosphorylation of Ser-262 and it also was involved in the phosphorylation of Ser-356[35, 36]. Interestingly, it has been demonstrated that the Tau phosphorylation at these sites is correlated with tau detachment from microtubules but not with tau aggregation. In fact, it is a common assumption that because the phosphorylation is necessary for weakening the Tau-microtubule interaction it also drives the Tau aggregation. However, several studies showed that this aggregation is more likely driven by the presence of polyanions or polycations than by the phosphorylation itself[37, 38, 39].

In total five protein phosphatases were found: PP1, PP2A, PP2B, PP2C and PP5. Among all of these, PP2A accounts for 70% of the phosphatase activity[40]. However, PP2A was found downregulated in **AD** brain[41, 42] mainly because an up-regulation of its inhibitors I_1^{PP2A} and I_2^{PP2A} [43, 44]. I_2^{PP2A} inhibits PP2A after being cleaved by Asparaginyl Endopeptidase in two smaller active fragments[45]. Another factor implicated in the downregulation of PP2A is the apolipoprotein E whose expression is the main genetic risk in **AD**[46]. PP2A was shown to dephosphorylate almost all the sites phosphorylated by the kinases involved[21] and, in addition, it regulates the activity of several kinases. For example, its inhibition was found to up-regulate **CaMKII** activity, leading to hyperphosphorylation of Tau[47]. On the contrary, its inhibition was correlated with the inhibition of **GSK3 β** by phosphorylation at Ser-9[48]. Interestingly, PP2A is found downregulated in many Tau hyperphosphorylation cases observed. **AD** animal models showed an increase of hyperphosphorylated tau in hypothermia conditions. This phenomenon was often correlated with inhibition of PP2A activity[49, 50, 51]. Interestingly, inhibition of PP2A and the consequent accumulation of hyperphosphorylated Tau was observed also during the sleep[52] and after anaesthesia[53].

1.3.1 Kinases and Phosphatases as drug targets

In light of the above considerations, kinases and phosphatases are considered potential targets for the design of an effective therapy for **AD**. Most of the strategies consist of inhibitors of **GSK3 β** or activators of PP2A. Anyway, none of the clinical trials led to positive results. Among the **GSK3 β** inhibitors, the most known are the *tideglusib*, *lithium* and the *valproic acid*[54, 55, 56]. All these compounds failed to

show significant cognitive improvement in Phase II. Anyway, during the last years, there has been a growing interest in the research in the development of **GSK3 β** inhibitors because of **GSK3 β** ubiquitous role in regulating several pathways. Typically, we can distinguish ATP-competitive or non-ATP-competitive inhibitors depending on if they bind to the ATP binding site. Currently, ATP-competitive inhibitors have been designed based on maleimide[57, 58], thiazolylureas[59] and paullones[60, 58]. Other compound families investigated as **GSK3 β** inhibitors are Indole derivatives, Pyrazolamide derivatives, Pyrimidine and Furopyrimidine derivatives, Oxadiazole derivatives and so on. For a complete list of these inhibitors see [58]. More recently, taking into account the incredible number of factors involved in **AD**, research shifted to a multi-target approach through which a single compound should be able to regulate more targets[61, 62]. For example, Cavalli et al. designed an inhibitor for **GSK3 β** and BACE-1, which is a transmembrane protease implicated in **A β** generation[63].

Inhibition of PP2A has been tried to prevent by targeting its two inhibitors, I_1^{PP2A} and I_2^{PP2A} , or by targeting the lysosomal enzyme asparagine endopeptidase. Anyway, although PP2A is a promising target for drug design against **AD**, there are few drugs that have been actually tested.

1.4 Temperature and Alzheimer's disease

One of the main factors that are currently being studied in order to find an explanation for Alzheimer's disease development is Temperature. The studies started by observing increased hyperphosphorylation of Tau in the brains of starving animals. Yanagisawa et. al was the first to describe this phenomenon in 1999 by applying food deprivation to mice for 1 to 3 days[64]. They showed that the subsequent Tau hyperphosphorylation that followed the starvation was due to the increased activity of several kinases, but they were still not able to explain what was happening at a molecular level. In further studies, Planel et. al deep into this phenomenon[49]. They showed for the first time that alteration of glucose metabolism led to increased tau hyperphosphorylation by an induced lowering of the body temperature. So, for the first time, a link between hypothermia and tau hyperphosphorylation was shown. In particular, some of the most interesting pieces of evidence of this phenomenon are: hypothermia alone was sufficient to induce tau hyperphosphorylation in acute brain slices and tau phosphorylation was completely restored to control values by maintaining the animals to normothermia. Also, some hypotheses on how hypothermia is a driven factor of Tau

hyperphosphorylation were formulated. In particular, a different inhibition of kinases and phosphatase activity was observed, with the former deactivated linearly and the latter exponentially. During the same years, Arendt et. showed also a direct correlation between hibernation and tau hyperphosphorylation[65]. These introductive works led to an increased investigation of the role of hypothermia on Alzheimer's disease development and a decreased body temperature was definitely recognized as a risk factor[66]. In particular, some conditions that could lead to hypothermia were elucidated. Ageing is the main risk factor that is associated with Alzheimer's disease and is also associated with hypothermia. Elderlies regulate body temperature less efficiently than younger people, this could explain why they are more subjected to Alzheimer's disease. In addition, elderlies are more subjected to metabolic diseases, such as *Diabetes Mellitus*, whose typical outcome is hypothermia. Hypothermia can be also an outcome of anaesthesia, as demonstrated by several studies.

In 2011, Arendt et. al tried to investigate which kinases and phosphatases are more influenced by hypothermia conditions[67]. In particular, they focused the analysis on three species: arctic ground squirrels, Syrian hamsters and black bears. Of course, all the conditions that are described by the study are physiological because all these three animals are hibernators, so all the changing in the activation levels of kinases and phosphatases that has been observed, as well as the changing of the Tau phosphorylation levels, have to be considered physiological and totally reversible when the hibernation condition stop. First of all, they showed that a lower body temperature induces specific phosphorylation of Tau and not of other potential phospho-proteins. So, hibernation is a triggering factor for a protective physiological mechanism that has still to be elucidated. They showed increased phosphorylation of some Alzheimer's disease-related phospho-sites such as T231, S235, T212, S214, T217. It is interesting to notice that, although **GSK3** is considered one of the main kinases that drive the development of Alzheimer's disease, in this study it is found inhibited through phosphorylation at S9. This can be explained by remembering that this study refers to *physiological conditions*, and so the mechanism that it is shown should be considered normal. On the contrary, in Alzheimer's disease, although it is observed a Tau hyperphosphorylation, in some way differs from the one observed in this study because it is irreversible. However, in the study, increased activation of cdk5 and ERK1 (p44) has been observed. Along with **GSK3**, it has been observed the inhibition of SAPK/JNK and ERK2 (p42). It is worth noting that the study has not focused on PP2A levels of activation or inhibition, which are considered pivotal in Alzheimer's disease and most likely the main factor that drives Tau hyperphosphorylation.

1.4. TEMPERATURE AND ALZHEIMER'S DISEASE

One of the first works that highlighted the link between temperature and PP2A activity was performed by Liu et. al in 2015[68]. In particular, they focused on the phosphorylation of several proteins in postmortem tissues, before and after perfusion with an ice-cold buffer.

Several other studies showed the link between temperature and hyperphosphorylation of tau[69, 70], and in 2020 for the first time, it is shown, by using animal models, a link between tau phosphorylation and sleep[52]. They showed for the first time that tau phosphorylation undergoes sleep-driven circadian variations. More interestingly, they demonstrated that this sleep-modulated phosphorylation of Tau is driven by changes in Temperature that induce inhibition of PP2A. This article for the first time highlights in humans a physiological mechanism that is currently unknown and that appears as the main metabolic mechanism whose defects drive Alzheimer's disease pathology. Under this light, Tau phosphorylation can not be considered a pathologic mechanism, but more as a neuroprotective mechanism that is triggered in the body by lowering the temperature in a specific situation, such as sleep, and if is triggered in wrong situations led to the development of neurodegenerative diseases such as Alzheimer's disease. In 2022, the first study that correlates temperature to Tau pathology in humans was published[71].

2

Computational Methods

2.1 Structures

All the work has been performed using a structure (PDB: 7PQC) composed of 14 tubulins, a segment of Tau Protein (from 202 to 395 residue), 7 GDPs, and 7GTPs. The structure was obtained through electron microscopy and presented a resolution of 4.10 Å. The initial structure presented bovine beta-tubulins so, it was modified with MOE in order to obtain a human system. In particular, human β 3-tubulin was added to the structure by substituting the initial β -tubulin through homology modelling. In addition, MOE was used for adding phosphorylate groups to the twenty serines of the Tau segment. In this way, four structures were achieved, respectively called: 7PQC, 7PQC_H, 7PQC_P and /7PQC_HP. After performing the analysis on these structures, it was decided to investigate the influence of melatonin on the modulation of Tau-microtubule binding. So, four additional structures with seven melatonin, one for each dimer, collocated in specific sites identified by the MOE site finder were created.

2.2 Molecular Operating Environment

The Molecular Operating Environment (MOE) tool allows a combination of visualisation and manipulation of atomic structures. It was used for three reasons:

- Structure manipulation
- Homology modelling
- Molecular Docking

MOE is the tool selected for manipulating the structures. It allows for a change of aminoacidic sequences of the structure, the protonation state and the phosphorylation state. All the structures have been prepared using the MOE QuickPrep tool by selecting a 7.4 pH and the PROPKA algorithm for defining the protonation state of the aminoacids. MOE includes a site finder tool that allows the identification of potential binding sites by analysing the geometry of the structure.

2.2.1 Homology modelling

MOE was used in order to construct new structures that more resembled the human tubulin. In particular, looking at the aminoacidic sequence of the β -tubulins of 7PQC can be observed that is from a bovine source. So, through homology modelling has been substituted the former β -tubulin with the human β 3-tubulin, which was chosen because is the most abundant tubulin isotype in the human brain. The process for substituting the β -tubulin of the initial structure with human β 3-tubulin can be divided in three steps: template selection, alignment and model construction. The sequence of β 3-tubulin was found on the UniProt database. Fortunately, β -tubulin structure is well studied and so MOE found several potential templates for constructing the new model. So, after having identified the potential template structure, an alignment and a subsequent superposition were performed. It is worth noting that, because the tubulin C-terminal is a highly disordered sequence, this procedure fails to find a good template for this segment and so assigns it a defined three-dimensional structure.

2.3 Molecular modelling

Molecular modelling refers to all the theoretical and computational techniques that are developed and used to investigate the molecular system and extract informa-

tion about its behaviour in different conditions, which can also resemble a pathological state. Typically, these techniques are applied to sub-cellular systems such as proteins, nucleic acids and membranes.

The number of particles that described a system can make sometimes be prohibitive to perform adequate analysis on a system, because of the computational resources that are needed. Molecular modelling starts with the physical description of a system, which can change depending on the scale that is used to describe it. The lower the scale, the better will be the description of the system and the higher will be the resources needed to perform the analysis.

The best description of a system can be achieved by working at the Quantum scale, in which each electron is modelled by a single particle. Anyway, this approach is too computationally expensive, because it assumes the solving of the Schrodinger equation, and can be used only for small systems or on small portions of a big system, such as active sites of an enzyme.

The most widely used approach is the Molecular Mechanics (MM) approach which consists of describing the system at the nanoscale by constructing particles that include a single atom or groups of atoms, for example including in a particle also the hydrogens of a heavy atom. The mass of these particles allows us to describe them with a certain precision, by using the Newton equation.

Both methods allow the extraction of macroscale properties by sampling the phase states of the system.

2.4 Molecular Mechanics

Molecular Mechanics allows extracting properties of the system by solving Newton's equation of motion. The energy of the system is described by the *Potential Energy Function* V which only depends on the relative positions of particles. The set of parameters that describe the system is called *Force Field* (FF)

2.4.1 Potential Energy Function

The Potential Energy Function is composed of the sum of two terms: *bonded interactions*, associated with the covalent bonds of two atoms, and *non-bonded interactions*, which are composed by electrostatic interactions and Van der Waals forces.

$$V = V_{bonded} + V_{non-bonded} \quad (2.1)$$

The bonded interaction can be divided into three terms: bond, angle and dihedral.

$$V_{bonded} = V_{bond} + V_{angle} + V_{dihedral} \quad (2.2)$$

The *bond term* refers to the energy components that derive from the presence of a covalent bond and depend on the distance between two particles that are implicated in the bond. The total energy of the bond term is given by the sum of all the contributions of the covalent bonds:

$$V_{bond} = \sum_{bonds} \frac{1}{2} K_{ij} (r_{ij} - r_{0,ij})^2 \quad (2.3)$$

where K_{ij} is the bond stiffness and $r_{0,ij}$ is the bond length at the equilibrium. Both parameters are included in the Force Field.

The *angle term* is described by the angle drawn by the reciprocal position of three atoms. It is modelled by a harmonic potential:

$$V_{angle} = \sum_{angles} \frac{1}{2} \xi_{ijk} (\theta_{ijk} - \theta_{0,ijk}) \quad (2.4)$$

where θ_{ijk} is the bond angle between atoms i, j and k , ξ_{ijk} is the angle stiffness and $\theta_{0,ijk}$ is the bond angle at the equilibrium. Also, these parameters can be found in the Force Field.

The *dihedral term* is described by four particles and refers to the rotation of a particle respected to a plane described by the other three. It takes into account for steric effect among atoms and can be modelled as a series of cosines:

$$V_{dihedral} = \sum_{dihedrals} \psi_{ijkl} [1 + \cos(n\phi_{ijkl} - \phi_{0,ijkl})] \quad (2.5)$$

where ϕ_{ijkl} is the dihedral angle between atoms i, j, k and l , ψ_{ijkl} is the dihedral stiffness and $\phi_{0,ijkl}$ is the dihedral angle at the equilibrium.

Non-bonded interactions can be divided into long-range interactions, which are the electrostatic interactions, and short-range interactions, which are the Van der Waals forces. Electrostatic interactions are modelled by the Coulomb law:

$$V_{Coulomb} = \frac{q_i q_j}{4\pi\epsilon_0\epsilon_r r_{ij}} \quad (2.6)$$

where ϵ_0 is the vacuum permittivity, ϵ_r the relative permittivity and r_{ij} the distance between the atoms i and j . Short-range interactions can be described by the Lennard-Jones 12-6 equation:

$$V_{vdW} = 4\epsilon_{ij} \left[\left(\frac{\sigma_{ij}}{r_{ij}} \right)^{12} - \left(\frac{\sigma_{ij}}{r_{ij}} \right)^6 \right] \quad (2.7)$$

r_{ij} is again the distance between the atoms i and j , σ_{ij} is the collision diameter, that is the interatomic distance where the Van der Waals potential is equal to zero, and ϵ_{ij} is the wall depth, such as the minimum of the Van der Waals forces. The positive term of the Lennard-Jones equation shows that atoms that come too close to each other are subjected to repulsive forces. This phenomenon is due to the overlap of the electronic clouds. By introducing all the terms in the initial formula it is possible to obtain a complete expression of the Potential Energy equation:

$$\begin{aligned} V = & \sum_{bonds} \frac{1}{2} K_{ij} (r_{ij} - r_{0,ij})^2 + \sum_{angles} \frac{1}{2} \xi_{ijk} (\theta_{ijk} - \theta_{0,ijk}) \\ & + \sum_{dihedrals} \psi_{ijkl} [1 + \cos(n\phi_{ijkl} - \phi_{0,ijkl})] + \\ & \frac{q_i q_j}{4\pi\epsilon_0\epsilon_r r_{ij}} + 4\epsilon_{ij} \left[\left(\frac{\sigma_{ij}}{r_{ij}} \right)^{12} - \left(\frac{\sigma_{ij}}{r_{ij}} \right)^6 \right] \quad (2.8) \end{aligned}$$

The *non-bonded interactions* are the ones that most of all affect the computational costs of the simulation. Their number increases as the square of the number of particles in the system. For this reason, several methods has been developed to decrease the computational costs of these interactions, such as *cut-off distance* method, *Shifted Potential* method, *Switched Potential* method, *Particle Mesh Ewald* and so on.

2.4.2 Periodic Boundary Conditions

In order to create a faithful representation of a physical system, typically the boundaries of the system are set and the *box* that is generated by this procedure is solvated. However, artefacts can be generated by the collisions of particles on the edge of the box. In these conditions, a box as big as possible would be needed, leading to a higher computational cost because of the increased number of solvent particles for filling the box. The best, and also most used, way to overcome this problem is using *Periodic Boundary Conditions*. The box, and so the entire system, is repeated in all directions giving the illusion of an infinite system. The particles of the system are allowed to jump on adjacent boxes, but this movement is repeated in all the other boxes. In this way, it is possible to eliminate the artefacts due to rigid

edges. However, this method allows to limit of the dimensions of the system but amplified the number of long-range interactions that should be calculated, making more necessary the use of one of the methods cited before such as the Particle Mesh Ewald.

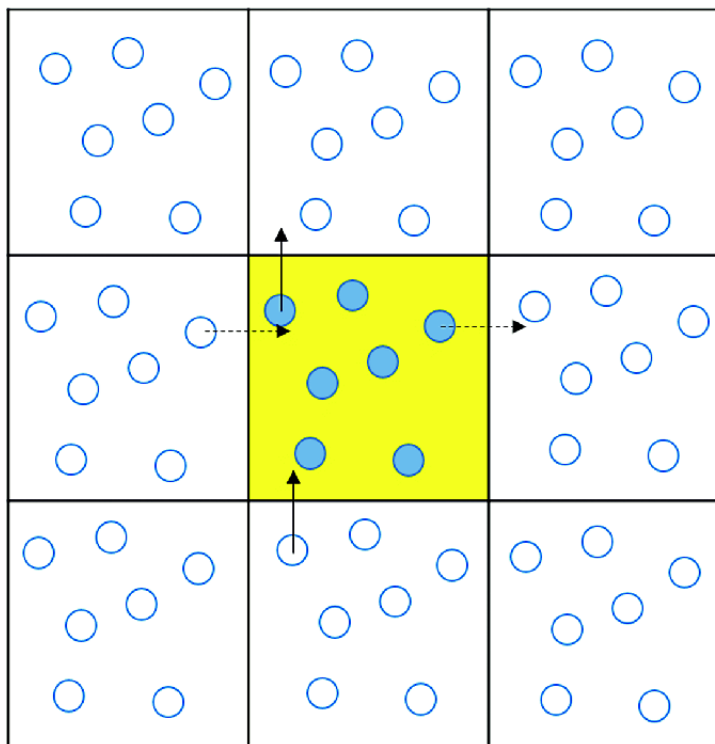


Figure 2.1: Two-dimensional representation of periodic boundary condition.

2.4.3 Potential Energy minimization

Potential Energy can be described by a multi-dimensional space with $3N$ coordinates, where N is the number of particles, called Potential Energy surface (PES).

Typically, a system, after its construction, is in a high-energy state. Performing a simulation in these conditions leads rapidly to failure because the forces applied to the particles would be too high. The force on each particle is described by the following law:

$$\vec{F} = -\nabla \cdot \vec{V} \quad (2.9)$$

This means that, in order to lower the forces on each particle, the atomic positions should be adjusted in order to move the system in low slope areas on the

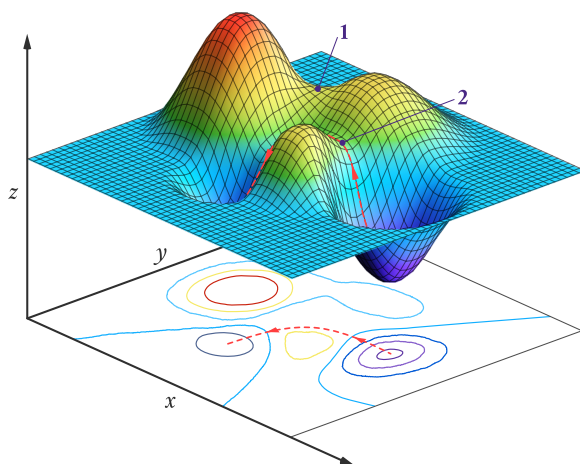


Figure 2.2: Representation of the Potential Energy surface.

potential energy surface. Low slope areas correspond to *minima points* on the energy surface and, they can be divided into *local minima* and *global minima*. Energy minimization is a set of techniques that allows a slight adjustment of the atomic positions in order to find a minimum point, typically the nearest one. We can also distinguish two sub-families of minimization techniques: *derivative methods* and *non-derivative methods*. The first ones are further divided into *first order methods*, such as Steepest Descent and Conjugate Gradient, and *second order methods*, such as Newton-Raphson and LBFGS.

2.5 Molecular Dynamics

Molecular Dynamics (MD) refers to a computational technique that aims to study the evolution of a system in time. It is applied to systems at the nanoscale or bigger. By calculating a trajectory of a system, it is possible to infer macroscopic properties such as temperature and free energy.

2.5.1 Statistical ensemble

The concept of an ensemble was introduced by J. Willard Gibbs in 1902. An ensemble is a collection of a large number of indistinguishable replicas of the system under consideration, which interact with each other, but are isolated from the rest of the universe. The replicas could be in different microscopic states, as determined by the positions and momenta of the constituent molecules, for example,

but the macroscopic state determined by the pressure, temperature and/or other thermodynamic variables are identical. So, an ensemble is a collection of different microstates that share identical microscopic properties. Each microstate represents a point of the *phase space*. Molecular Dynamics allows to sample the phase state, each frame obtained with molecular dynamics is a microstate of the system. There are different types of ensemble:

- The Micro-Canonical Ensemble (NVE) corresponds to an isolated system and it is characterized by a fixed volume, energy and number of atoms;
- The Canonical Ensemble (NVT) corresponds to a closed system and it is characterized by a fixed volume, temperature and number of atoms;
- The Grand Canonical Ensemble (VT) corresponds to an open system and it is characterized by a fixed volume, temperature and chemical potential;
- The Isobaric-Ensemble (NPT) is characterized by a fixed pressure, temperature and number of atoms.

By collecting a large number of microstates that define a statistical ensemble, it is possible to calculate macroscopic properties:

$$\langle A \rangle_{ensemble} = \iint dp^N dr^N A(p^N, r^N) \rho(p^N, r^N) \quad (2.10)$$

where r is the atomic positions, p is the momenta, $A(p^N, r^N)$ is the property of interest and $\rho(p^N, r^N)$ is the probability density function. The probability density function is given by:

$$\rho(p^N, r^N) = \frac{1}{Q} \exp\{-H(p^N, r^N)/k_b T\} \quad (2.11)$$

where k_b is the Boltzmann factor, T is the temperature, H is the Hamiltonian and Q is the *Partition function*. The partition function is defined as:

$$Q = \iint dp^N dr^N \exp\{-H(p^N, r^N)/k_b T\} \quad (2.12)$$

Looking at the expression of the partition function, we can see that it represents the sum of Boltzmann factors over all the microstates. Boltzmann factors assume higher values in correspondence with low-energy microstates. So, the partition function defines the states that are easily accessible by the system. By solving the partition function would be possible to obtain all the possible microstates of the

system, however, this function is not analytically solvable. In order to solve this function, we can take advantage of the Molecular Dynamics method. Assuming valid the *ergodic hypothesis*, it is possible to equalize an average value calculated on time with the statistical average value defined previously.

$$\langle A \rangle_{time} = \lim_{\tau \rightarrow \infty} \frac{1}{\tau} \int_{t=0}^{\tau} A(p^N(t), r^N(t)) dt \simeq \frac{1}{M} \sum_{t=1}^M A(p^N, r^N) \quad (2.13)$$

So, with a long simulation is possible to collect enough microscopic states to make the time average tend to the statistical average.

2.5.2 Molecular Dynamics implementation scheme

Molecular Dynamics integrates Newton's motion equations in order to obtain a trajectory that describes the evolution of a physical system in time. Each frame of the trajectory contains three spatial coordinates and three velocity values for each particle. For each particle, we can define the acceleration that it feels as the opposite of the potential energy gradient:

$$a = -\frac{1}{m} \frac{dv}{dr} \quad (2.14)$$

However, the potential energy function is too complex to be solved analytically and so, it is necessary to implement numerical methods for solving the motion equations. firstly, it is necessary to choose an appropriate time-step, that is typically 1/10 of the minimum oscillation period of the system, which corresponds to the oscillation period of a covalent bond. At this point, there are several choices as possible integration algorithms, the most used are Verlet, Leap-frog and Velocity Verlet.

2.3 shows a scheme of a Molecular dynamics algorithm. It starts by defining the initial positions of the particles and the time step. After that, potential energy is calculated and so are the forces acting on each particle. Then, from the forces is possible to calculate acceleration and the new position e velocity values for each particle. This process continues until the maximum number of steps is reached.

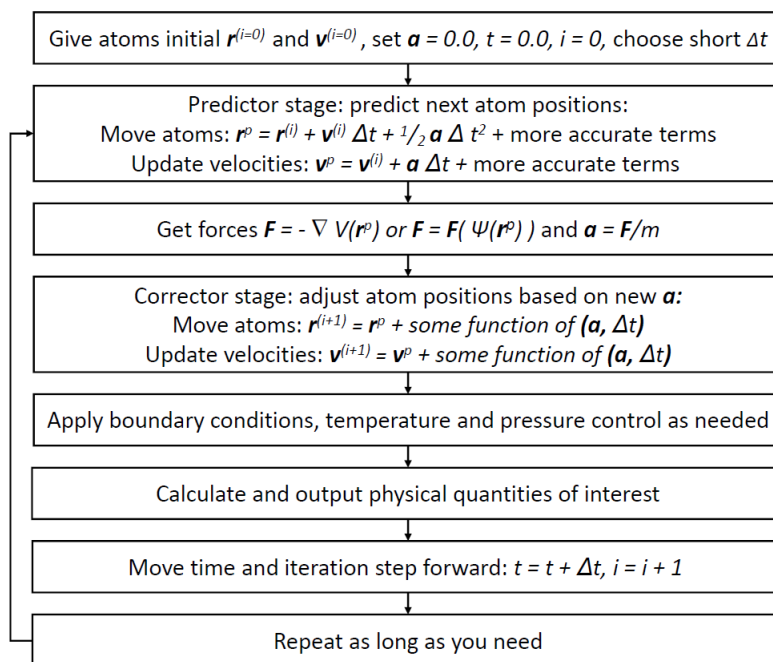


Figure 2.3: Simplificated scheme of a Molecular Dynamics algorithm

2.6 Binding free energy prediction

Typically, one of the most important macroscopic properties that are calculated during the study of a biological system is the *Binding Free Energy* of two molecules. The standard binding free energy is defined as:

$$\Delta G^0 = \Delta H^0 - T\Delta S^0 = -RT \ln K_i \quad (2.15)$$

where H is the enthalpy, S is the entropy, T is the absolute temperature, R is the gas constant and the superscript "0" means that the binding free energy is evaluated at standard conditions. The Molecular Mechanics/Poisson-Boltzmann Surface area (MM/PBSA) and Molecular Mechanics/Generalized-Born Surface Area (MM/GBSA) methods are the most used for estimating binding free energy values. They are "implicit solvent" methods, so they approximate the solvent with a continuum medium. These methods define the free binding energy of one receptor and a ligand as:

$$\Delta G_{bind} = \langle G_{PL} \rangle - \langle G_P \rangle - \langle G_L \rangle \quad (2.16)$$

where G_{PL} is the energy of the complex, G_P is the energy of the receptor and G_L is the energy of the ligand.

However, a typical approach consists of simulating the complex and extracting the free receptor and free ligand trajectories by simply eliminating the appropriate atoms. In this way, the previous expression will be:

$$\Delta G_{bind} = \langle G_{PL} - G_P - G_L \rangle_{PL} \quad (2.17)$$

The energy of each state (PL, P, L) is calculated according to the following formula:

$$G = E_{bnd} + E_{el} + E_{VdW} + G_{pol} + G_{np} - TS \quad (2.18)$$

where E_{bnd} includes the contributions of bonds, angles and dihedrals. E_{el} and E_{VdW} are the electrostatic and Van der Waals interactions. G_{pol} and G_{np} are respectively the polar and non-polar contributions. G_{pol} is obtained from the Poisson-Boltzmann equation or from the Generalized born model. G_{np} is estimated from a linear relation to the solvent-accessible surface area (SASA):

$$\Delta G_{non-polar} = \gamma SASA + b \quad (2.19)$$

2.7 Molecular Docking

Molecular Docking refers to a set of low computationally expensive techniques used to obtain an estimation of the stability of a receptor-ligand complex. In order to perform such a procedure, the following programs have been used:

- AutoDock
- Autodock Vina
- MOE

2.7.1 Consensus docking

The accuracy of the docking procedure strongly depends on the method used and the system that is investigated. In order to improve the accuracy, a well-studied pipeline consists of using different programs to perform the same docking and compare the results. Poses obtained by more programs are most likely to be the most probable ones. Autodock, AutoDock Vina and MOE predict the correct protein-ligand complex with an estimated accuracy of respectively 55%, 64% and

45%. The use of a combination of these three programs, and so of three different scoring algorithms, allows an increment of the scoring by 25-30%. After the docking process, a *rescoring* procedure has been carried out using AutoDock Vina. Following, the complete pipeline can be found:

1. Preparation of the ligands
2. Preparation of the targets
3. Identification of binding sites
4. Setting of methods' parameters
5. Consensus Docking
6. Results extraction

2.8 Electrostatic profile

In order to study the electrostatic profile of the structure, the pdb2pqr tool was used[2]. pdb2pqr allows to include in a pdb file the information regarding the charges in particular conditions, such as particular pH values.

The pdb2pqr pipeline starts by identifying potential problems in the structures, such as missing heavy atoms. If it finds missing heavy atoms, it reconstructs them. The reconstruction included also a "debump" process which checks that the new heavy atoms are not overlapped with the already existing ones. This process is performed by calculating the Van der Waals radii of the nearby atoms. After this check, hydrogens are added to the structure. Finally, atomic charges are assigned to the structure from the chosen force field. In this work, the AMBER force field was selected. In order to visualise the electrostatic map of the structure the Adaptive-Poisson Boltzmann solver (APBS) [72] has been used. It solves the Poisson-Boltzmann equation for large biomolecular assemblages.

$$\delta = -\nabla\epsilon\nabla\phi - \sum_i^M c_i q_i e^{-\beta(q_i\phi + V_i)} \quad (2.20)$$

The equation describes the electrical potential for M ionic species, which are described by their charges q_i , concentrations c_i , and steric ion-solute interaction potential V_i . ϵ is a dielectric coefficient. β is the inverse thermal energy. The tool can be used through their web-servers[73] which also incorporate the pdb2pqr

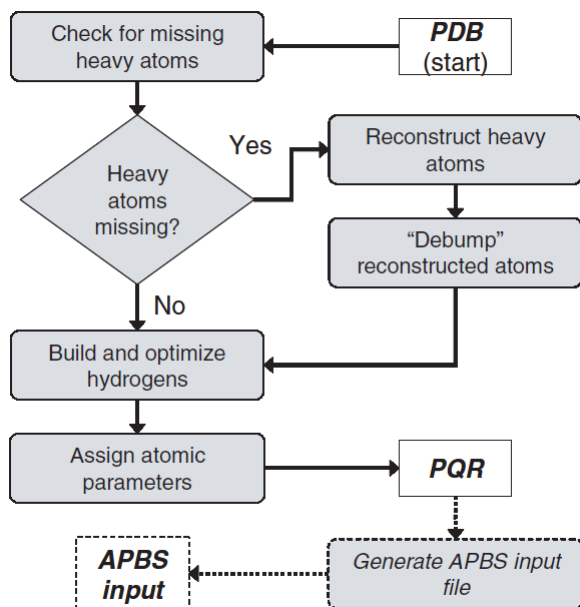


Figure 2.4: Flowchart demonstrating the sequence of operations performed by the pipeline. The process begins with an input PDB file and ends with a parameterized PQR file and, optionally, an APBS input file.[2]

pipeline. The web interface allows the selection of pH, Force field and output naming scheme for generating the pdb2pqr file. APBS has been used through PyMOL, which is a visualisation tool mostly developed with Python. PyMOL included an extension that allows using the APBS web server and visualises the result directly inside the PyMOL visualisation environment.

3

Results and discussion

3.1 Electrostatic maps

The electrostatic maps of the structure were constructed using the procedure explained in the previous section.

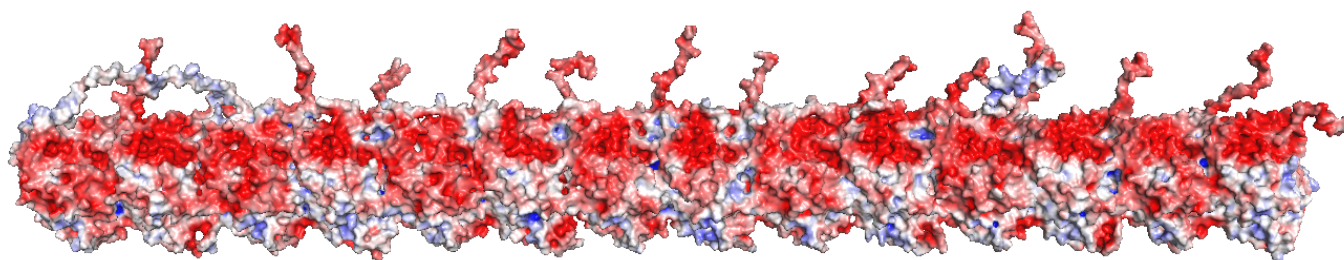


Figure 3.1: Electrostatic map of the structure, front view

Looking at the electrostatic maps it is easy to see that MAP Tau is located in a zone with a highly negative charge. This is in accord with the literature, where it can be found strong evidence that Tau phosphorylation makes Tau detach from the microtubules. The following, details on the location of Tau serines are shown:

Looking at the details of the serines' electrostatic maps, it is possible to note that they are located near regions with a strong negative charge. In addition, non-

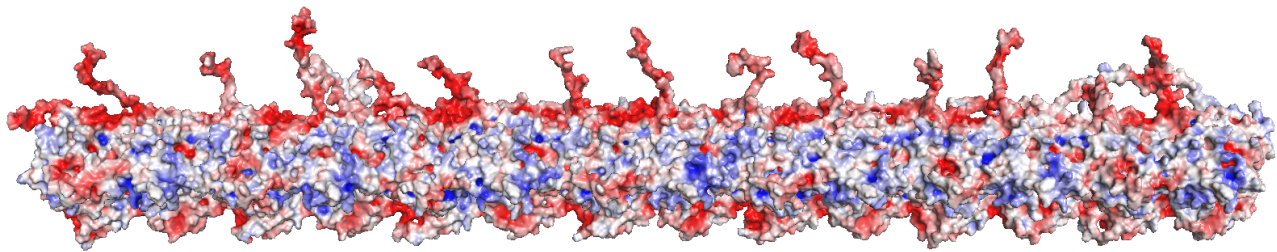


Figure 3.2: Electrostatic map of the structure, side view

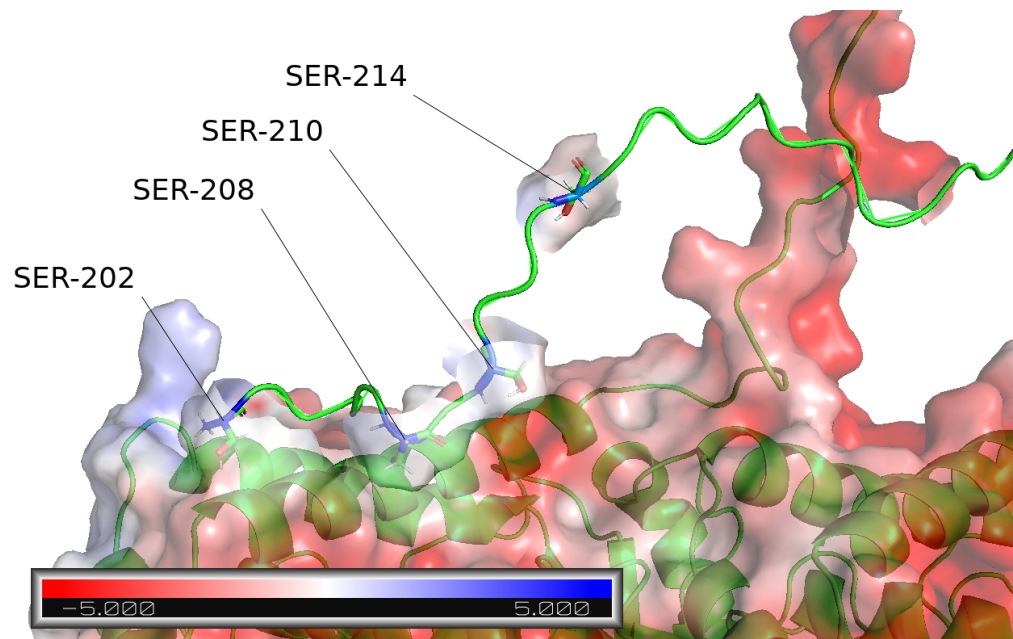


Figure 3.3: Electrostatic map of SER202, SER208, SER210, SER214

phosphorylated serines have a slightly positive charge that makes them prone to interact with the negative regions of the microtubule.

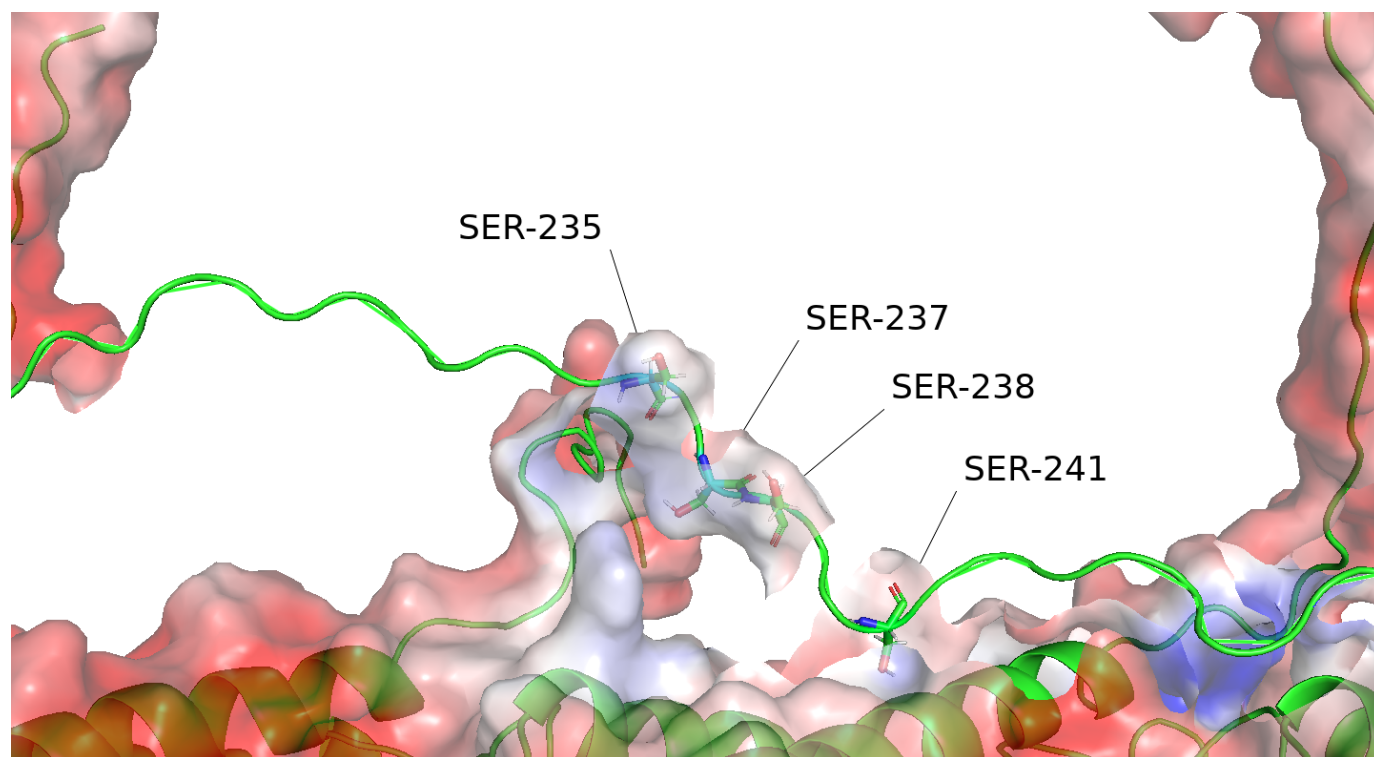


Figure 3.4: Electrostatic map of SER235, SER237, SER238, SER241

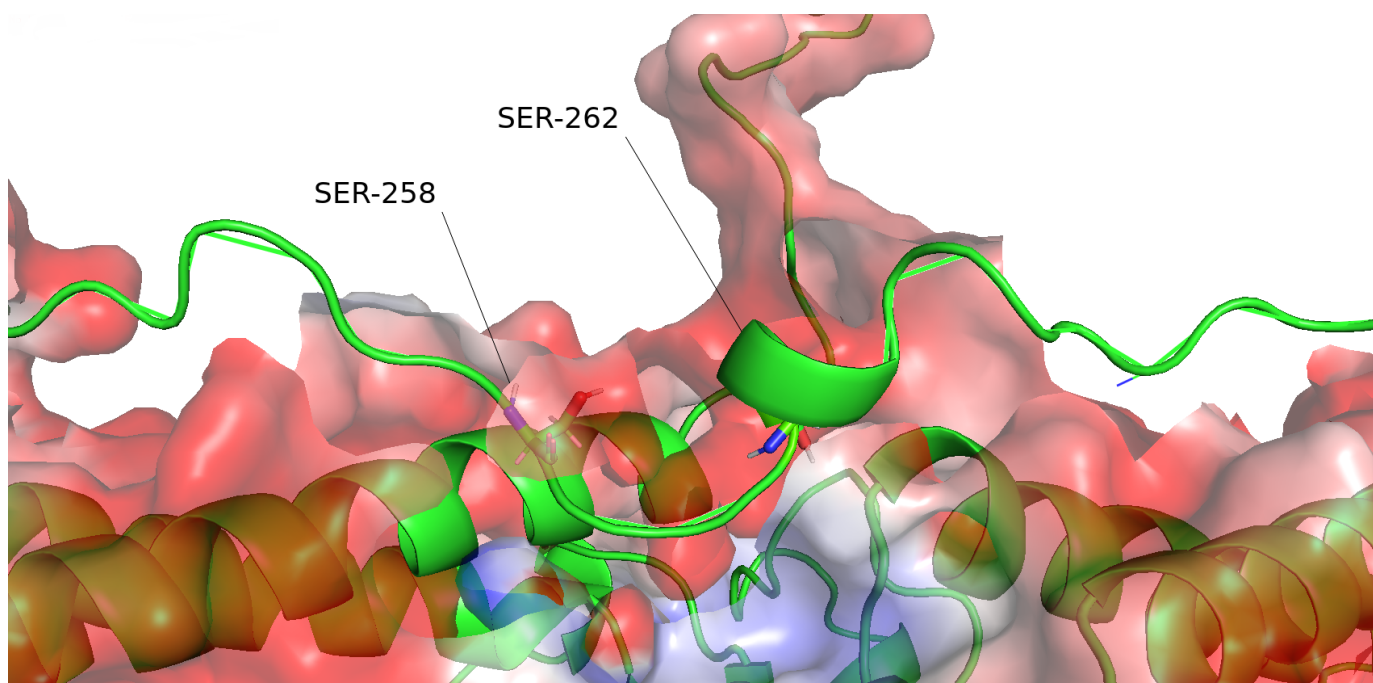


Figure 3.5: Electrostatic map of SER258, SER262

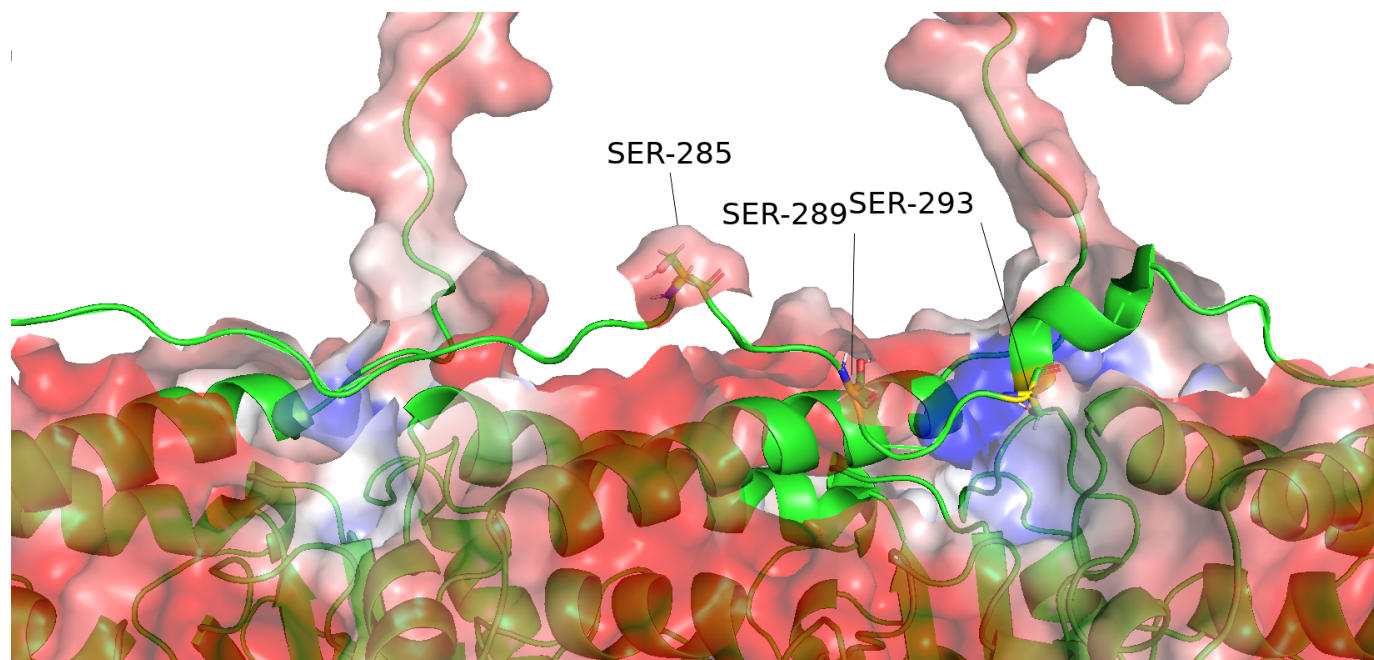


Figure 3.6: Electrostatic map of SER285, SER289, SER293

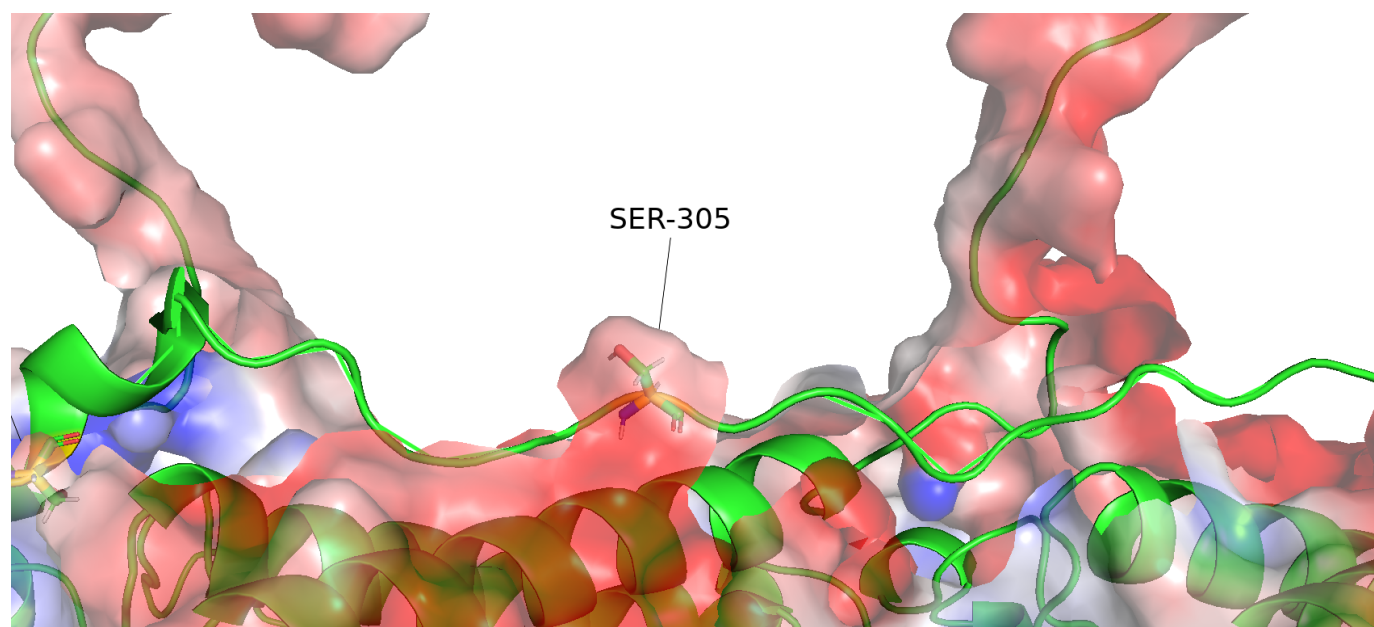


Figure 3.7: Electrostatic map of SER305

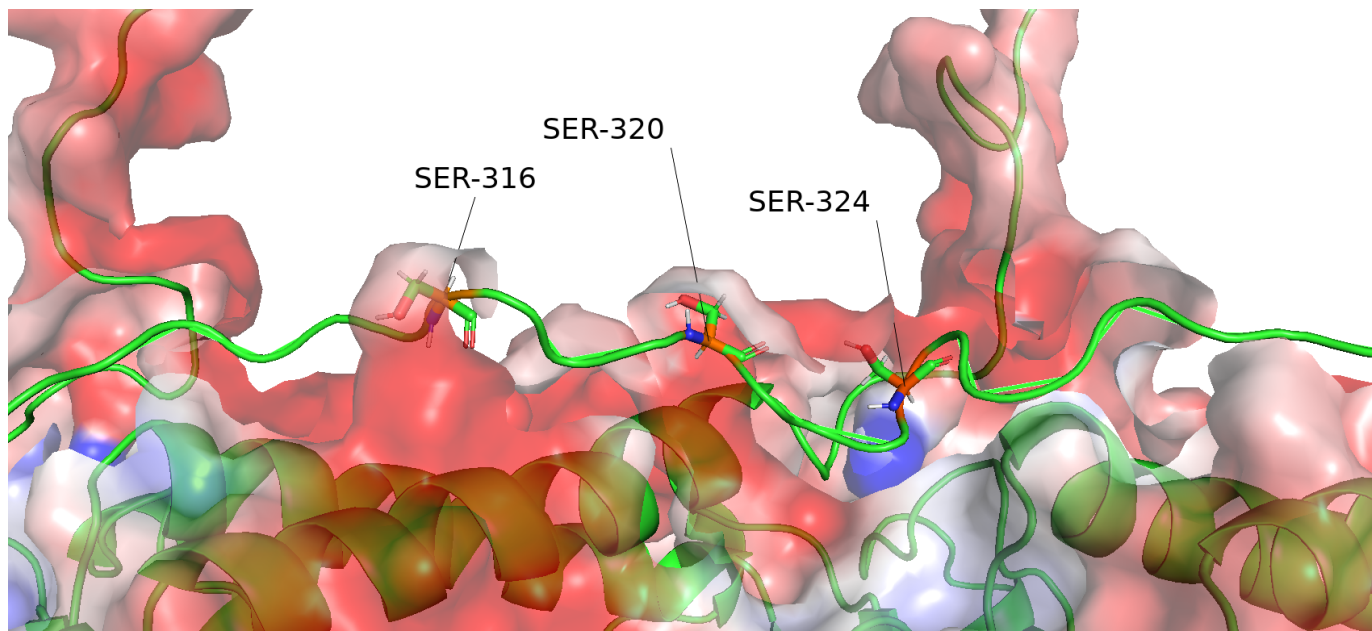


Figure 3.8: Electrostatic map of SER316, SER320, SER324

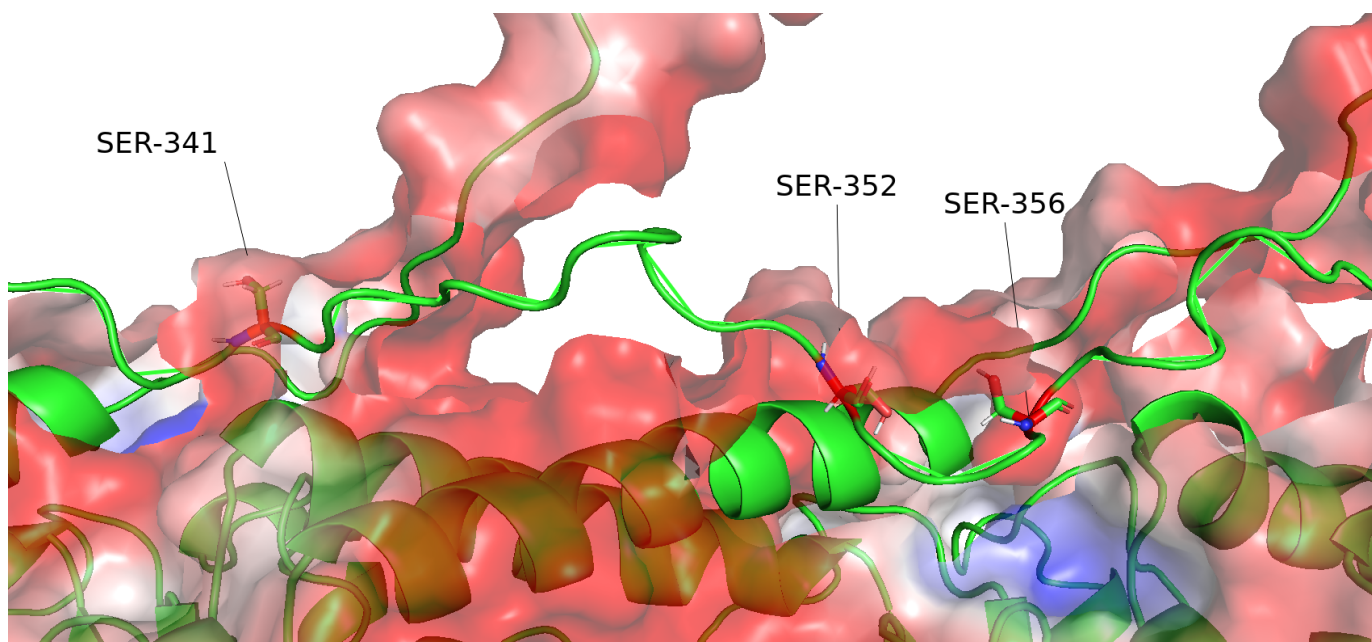


Figure 3.9: Electrostatic map of SER341, SER352, SER356

3.2 Molecular Dockings

In order to construct the four structures that include the melatonin, molecular docking was performed. The literature lacks information regarding a potential binding site of melatonin on microtubules. So, firstly, possible binding sites were found using the MOE site finder for both human and non-human structures. In particular, the structures were divided into seven dimers and a binding site was found for each dimer. Unfortunately, the site-finder identifies also binding sites that overlap with the GTP/GDP binding site. So, the binding sites that do not overlap were manually identified by looking at them with MOE. In the following tables can be seen the PLB value for every potential binding site identified for each dimer. In particular, the following workflow was followed:

1. Firstly, the 7 dimers were extracted from the structure.
2. Then, for each dimer, possible sites were extracted using the MOE site finder. All the dimers were exactly the same but, because they had slightly different conformations, the Site Finder found different binding sites for each one of them.
3. After that, consensus docking was performed (with Autodock, MOE and Vina) and for each site the best pose was extracted.
4. For each pose, a 100 ns simulation was performed
5. Then, MMGBSA was done on 1000 frames to evaluate the binding energy and the best site considering all the sites of all the dimers was found.
6. The final structure was built by adding the melatonin in that site in each dimer.

After the identification of the potential binding sites, consensus docking was performed using Autodock, Autodock vina and MOE. Following, the scores can be found:

After having identified potential binding sites, melatonin was added to each dimer and free-binding energy was estimated by a 100 ns simulation followed by MM/GBSA.

Table 3.1: PLB values, Not-Human structure. Bold values indicate binding sites that do not overlap with the GTP/GDP binding site.

Dimer1	Dimer2	Dimer3	Dimer4	Dimer5	Dimer6	Dimer7
3.55	4.53	3.35	2.97	2.99	3.80	4.34
2.38	2.08	2.66	2.62	2.54	3.62	2.71
2.30	1.76	2.33	1.94	1.76	1.53	1.98
1.87	1.71	1.64	1.43	1.65	1.20	1.60
1.45	1.68	1.58	1.43	1.57	1.14	1.40
1.41	1.04	0.67	1.42	1.27	/	1.12
1.16	/	0.55	1.17	1.13	/	1.07
1.15	/	/	1.10	1.00	/	/

Table 3.2: PLB values, Human structure. Bold values indicate binding sites that do not overlap with the GTP/GDP binding site.

Dimer1	Dimer2	Dimer3	Dimer4	Dimer5	Dimer6	Dimer7
3.43	2.52	3.31	5.31	2.36	4.21	3.76
2.83	2.34	2.62	1.93	2.20	2.40	3.55
2.24	2.30	2.08	1.06	1.65	1.80	0.77
1.57	1.64	1.49	/	1.45	1.01	/
1.52	1.37	1.17	/	1.33	0.74	/
1.31	1.34	1.10	/	1.31	0.64	/
0.72	0.90	/	/	1.25	0.64	/
/	0.77	/	/	1.22	0.61	/
/	0.70	/	/	1.05	/	/
/	/	/	/	1.01	/	/

3.2. MOLECULAR DOCKINGS

Site	Rescoring Vina	Consensus Score	Software
site1	-5.285	-5.212	moe
site2	-5.701	-5.790	autodock
site3	-6.059	-6.700	vina
site4	-5.710	-5.625	moe
site5	-7.003	-7.500	vina
site6	-5.499	-5.500	autodock
site7	-5.149	-6.220	autodock
site8	-6.108	-6.300	vina

Table 3.3: Docking results, dimer1 non-human

Site	Rescoring Vina	Consensus Score	Software
site1	-6.795	-7.400	vina
site2	-6.420	-6.140	autodock
site3	-5.219	-6.300	vina
site4	-5.686	-6.340	autodock
site5	-5.388	-5.900	vina
site6	-5.226	-5.338	moe

Table 3.4: Docking results, dimer2 non-human

Site	Rescoring Vina	Consensus Score	Software
site1	-6.525	-6.131	moe
site2	-6.476	-6.110	autodock
site3	-5.252	-5.600	vina
site4	-5.291	-5.740	autodock
site5	-6.134	-6.200	vina
site6	-5.904	-6.510	autodock
site7	-7.515	-7.800	vina

Table 3.5: Docking results, dimer3 non-human

Site	Rescoring Vina	Consensus Score	Software
site1	-7.402	-6.674	moe
site2	-7.409	-6.550	autodock
site3	-6.607	-7.800	vina
site4	-4.864	-5.200	vina
site5	-5.825	-6.000	vina
site6	-6.355	-6.490	autodock
site7	-5.676	-5.900	vina
site8	-7.036	-6.687	moe

Table 3.6: Docking results, dimer4 non-human

3.2. MOLECULAR DOCKINGS

Site	Rescoring Vina	Consensus Score	Software
site1	-7.201	-6.180	autodock
site2	-7.079	-6.730	autodock
site3	-6.566	-6.920	autodock
site4	-5.651	-6.310	autodock
site5	-6.034	-6.500	vina
site6	-5.792	-6.130	autodock
site7	-5.508	-6.000	vina
site8	-6.190	-6.006	moe

Table 3.7: Docking results, dimer5 non-human

Site	Rescoring Vina	Consensus Score	Software
site1	-7.212	-6.390	autodock
site2	-6.182	-7.340	autodock
site3	-5.777	-6.000	vina
site4	-5.309	-5.900	vina
site5	-6.027	-6.300	vina

Table 3.8: Docking results, dimer6 non-human

Site	Rescoring Vina	Consensus Score	Software
site1	-7.118	-7.400	vina
site2	-6.335	-6.089	moe
site3	-5.035	-5.700	vina
site4	-5.890	-6.600	vina
site5	-5.512	-5.780	autodock
site6	-5.519	-6.100	vina
site7	-5.573	-6.000	vina

Table 3.9: Docking results, dimer7 non-human

Site	Rescoring Vina	Consensus Score	Software
site1	-5.905	-6.100	vina
site2	-5.649	-5.450	autodock
site3	-7.117	-7.070	autodock
site4	-6.004	-5.820	autodock
site5	-5.705	-6.000	vina
site6	-5.053	-5.100	vina
site7	-4.760	-5.560	autodock

Table 3.10: Docking results, dimer1 Human structure

3.2. MOLECULAR DOCKINGS

Site	Rescoring Vina	Consensus Score	Software
site1	-7.112	-7.700	vina
site2	-6.912	-7.000	vina
site3	-5.240	-6.300	vina
site4	-7.118	-7.400	vina
site5	-6.838	-6.410	autodock
site6	-6.027	-5.920	autodock
site7	-5.414	-5.900	vina
site8	-5.561	-5.800	vina
site9	-5.864	-6.200	vina

Table 3.11: Docking results, dimer2 Human structure

Site	Rescoring Vina	Consensus Score	Software
site1	-7.168	-7.700	vina
site2	-7.181	-7.300	vina
site3	-5.313	-5.630	autodock
site4	-5.906	-6.325	moe
site5	-6.309	-6.239	moe
site6	-6.001	-5.460	autodock

Table 3.12: Docking results, dimer3 Human structure

Site	Rescoring Vina	Consensus Score	Software
site1	-7.197	-7.800	vina
site2	-7.526	-7.900	vina
site3	-4.747	-5.300	vina

Table 3.13: Docking results, dimer4 Human structure

Site	Rescoring Vina	Consensus Score	Software
site1	-5.879	-5.621	moe
site10	-5.489	-6.000	vina
site2	-6.408	-6.600	vina
site3	-6.026	-6.300	vina
site4	-5.485	-6.000	vina
site5	-5.202	-5.600	vina
site6	-7.137	-7.400	vina
site7	-7.027	-6.600	vina
site8	-6.186	-7.500	autodock
site9	-6.068	-5.820	autodock

Table 3.14: Docking results, dimer5 Human structure

3.2. MOLECULAR DOCKINGS

Site	Rescoring Vina	Consensus Score	Software
site1	-6.189	-7.310	autodock
site2	-7.247	-7.700	vina
site3	-5.967	-7.450	autodock
site4	-4.803	-4.900	vina
site5	-5.856	-6.490	autodock
site6	-7.257	-7.600	vina
site7	-7.282	-7.800	vina
site8	-5.446	-5.600	vina

Table 3.15: Docking results, dimer6 Human structure

Site	Rescoring Vina	Consensus Score	Software
site1	-6.326	-6.500	vina
site2	-6.389	-6.400	vina
site3	-6.512	-6.325	moe

Table 3.16: Docking results, dimer7 Human structure

Table 3.17: Free-binding energy of the melatonin-dimer binding [kJ/mol, Non-human structure]

DIMER1	DIMER2	DIMER3	DIMER4	DIMER5	DIMER6	DIMER7
-10.2 ±4.1	-21.1 ±4.4	-19.8 ±3.5	-30.6 ±3.5	-24.7 ±4.9	-23 ±4.8	-22.3 ±4.3
-25.4 ±5.0	-28.1 ±2.8	-17.8 ±5.9	-29.4 ±3.9	-15.6 ±3.9	-30.6 ±2.5	-26.3 ±3.2
-20.6 ±2.8	-3.6 ±5.8	-15.4 ±3.2	-28.5 ±3.8	-29.8 ±3.3	-29.4 ±3.4	-12.4 ±9.6
-11 ±5.3	-22.4 ±3.4	-20.8 ±4.0	-14.4 ±3.7	-38.8 ±3.3	-11.4 ±3.3	-30.3 ±4.9
-27.7 ±4.5	-14.3 ±7.9	-24.1 ±3.2	-22.4 ±3.2	-25.8 ±6.1	-9.8 ±5.6	-9.9 ±6.6
-23.6 ±3.6	-17.2 ±3.4	-7.5 ±5.0	-19.9 ±3.4	-17.6 ±3.4	/	-9.6 ±4.5
-12.8 ±3.7	/	-27.8 ±7.1	-22.7 ±2.7	-21.9 ±3.3	/	-16.2 ±5.0
-19.6 ±3.2	/	/	-28.2 ±4.0	-29.8 ±3.5	/	/

Table 3.18: Free-binding energy of the melatonin-dimer binding [kJ/mol], human structure

DIMER1	DIMER2	DIMER3	DIMER4	DIMER5	DIMER6	DIMER7
-24.5 ±4.5	-21.2 ±4.0	-22.8 ±3.6	-21.9 ±4.0	-35.5 ±3.3	-21.2 ±6.3	-14.5 ±5.2
-10.8 ±6.5	-24 ±5.5	-24.3 ±4.2	-28.1 ±2.9	-21.1 ±3.7	-28.8 ±3.0	-28.4 ±2.9
-31.9 ±3.7	-16.8 ±4.7	-11.5 ±6.3	-14.5 ±7.8	-14 ±4.9	-28 ±4.5	-26.7 ±2.9
-21.4 ±3.4	-26.9 ±2.9	-12.9 ±5.4	/	-21.5 ±3.9	-11.2 ±6.5	/
-18.6 ±3.3	-22.3 ±5.2	-28.3 ±3.5	/	-14.3 ±4.4	-16.4 ±8.7	/
-14.4 ±3.6	-20 ±3	-18.8 ±3.5	/	-24.9 ±4.9	-20.6 ±4.0	/
-18.4 ±4.5	-15.5 ±3.9	/	/	-33.7 ±3.6	-9.72 ±7.1	/
/	-19.6 ±6.9	/	/	-29.6 ±3.8	-21.6 ±2.9	/
/	-16.11 ±5.3	/	/	-19.9 ±5.8	/	/
/	/	/	/	-21.8 ±9.2	/	/

3.3. MOLECULAR DYNAMICS RESULTS

In this way, it has been possible to select the best binding site of melatonin and to construct four new structures with seven melatonin each. The best site was the fourth one of dimer5. So melatonin was added to each dimer in that site.

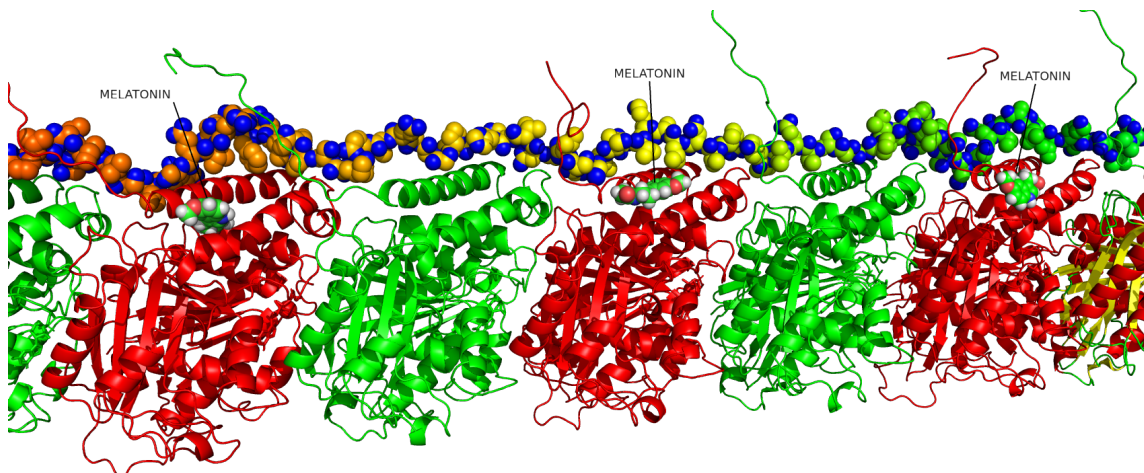


Figure 3.10: Detail of the structure with the melatonin inserted

3.3 Molecular Dynamics results

The Molecular Dynamics work was performed using the AMBER MD suite, which is, among GROMACS, one of the most popular and complete currently available. First of all, the system was prepared by using the *tleap* command. The *ff14SB* force field has been used to parameterize the proteins. TIP3P is the explicit water model chosen. GDP and GTP parameters were downloaded from the Manchester University database¹. Melatonin, if necessary, was parameterized with the GAFF force field. The system has been enclosed in a rectangular box with dimensions approximately of 115x120x620 Angstroms. The charge of the system has been neutralized and Na⁺ and Cl⁻ ions were added in order to reach a concentration of 0.15M.

After the construction of the eight structures, molecular dynamics simulations were performed. Firstly, the eight structures were subjected to two steps of minimization. The first minimization was performed by applying position restraints to the protein structure in order to minimize the water and the ions. Then 1000 steps

¹<http://amber.manchester.ac.uk/>

of steps descent followed by 1000 steps of the conjugate gradient were performed. The second step of minimization was performed by applying the position restraint to the water and the ions in order to minimize the protein structure. Also in this case, 1000 steps of the steepest descent and 1000 of the conjugated gradient were performed.

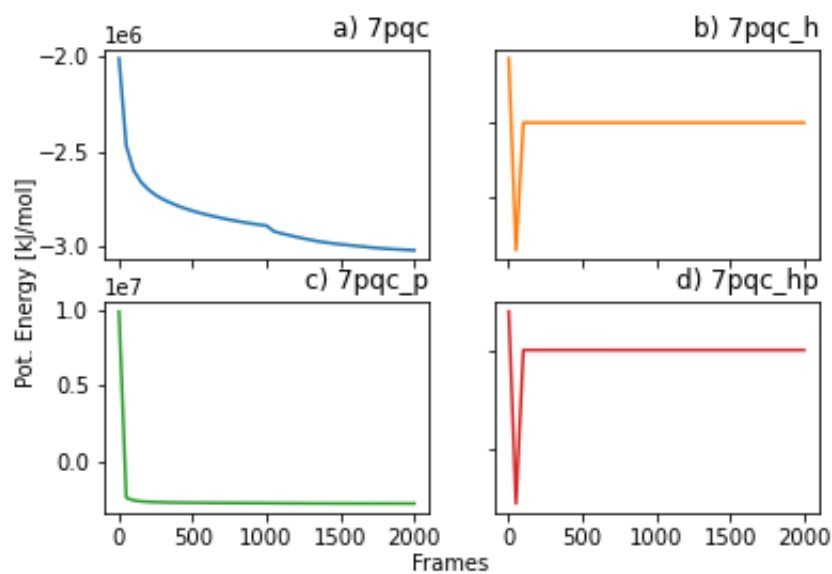


Figure 3.11: Minimization results, structures without melatonin

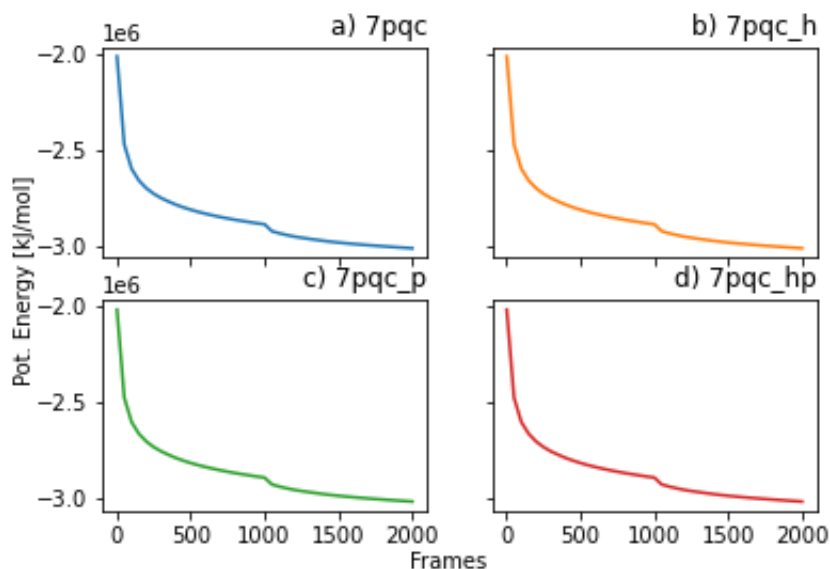


Figure 3.12: Minimization results, structures with melatonin

Then, the structure was equilibrated in an NVT ensemble for 1 ns with a time-step of 2 femtoseconds. As a thermostat, the weak-coupling algorithm was chosen. The system was equilibrated until 294 kelvins. Also, in this case, position restraints were applied to the proteins.

Finally, the system was equilibrated in NPT for 1 ns with position restraints applied to the proteins. The *Berendsen* barostat was chosen. The reference pressure was set to 1 bar and the pressure relaxation time to 1 ps. In this case, the *Langevin dynamics* was chosen as the thermostat, with a *collision frequency* of 1 ps^{-1} . 11 frames were extracted from the last 100 ps of the NPT equilibration and used to perform a simulation of 100 ns. In this simulation, the temperature was raised to 310 Kelvin with a Langevin dynamics thermostat. All the position restraints were removed. Following, the RMSD values of the 88 simulations are shown.

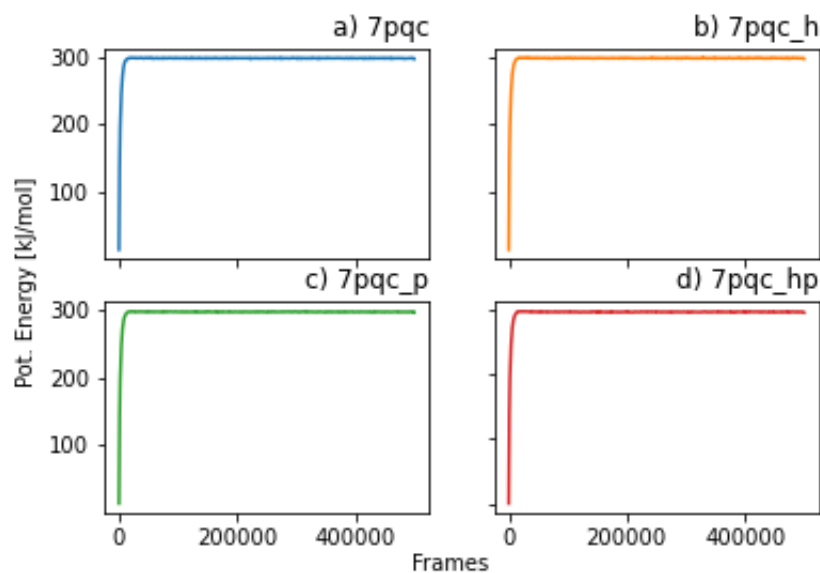


Figure 3.13: NVT equilibration, structures without melatonin

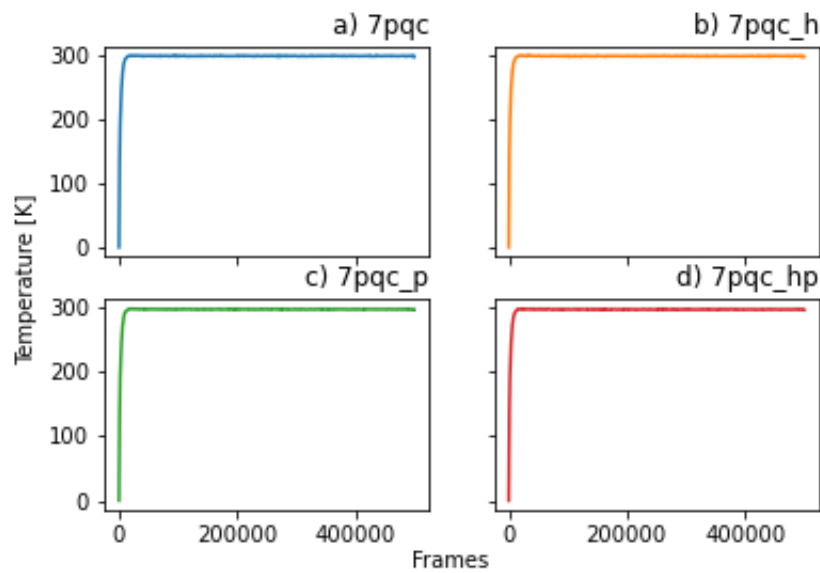


Figure 3.14: NVT equilibration, structures with melatonin

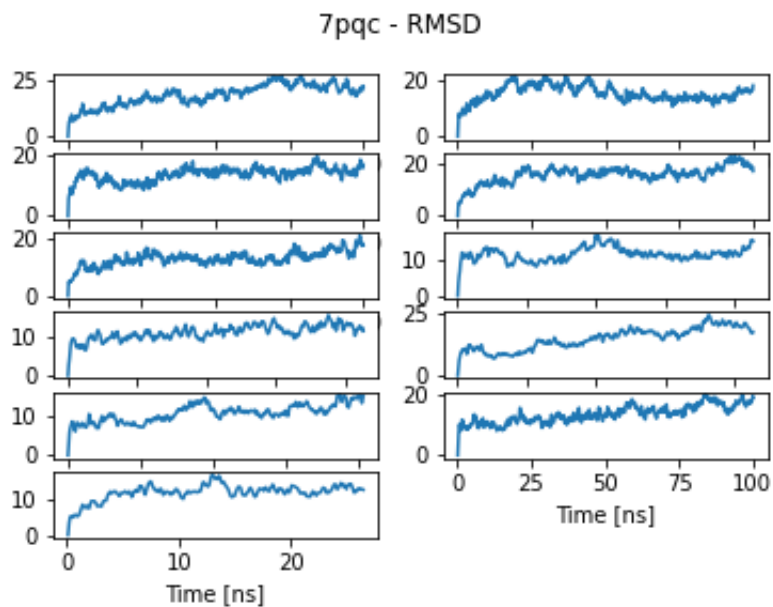


Figure 3.15: RMSD values, 11 simulations of 100ns, 7pqc

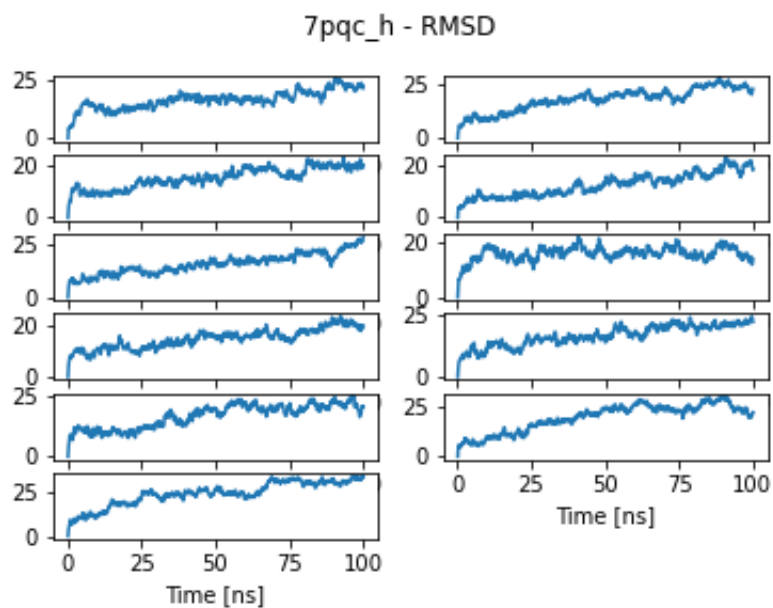


Figure 3.16: RMSD values, 11 simulations of 100ns, 7pqc human

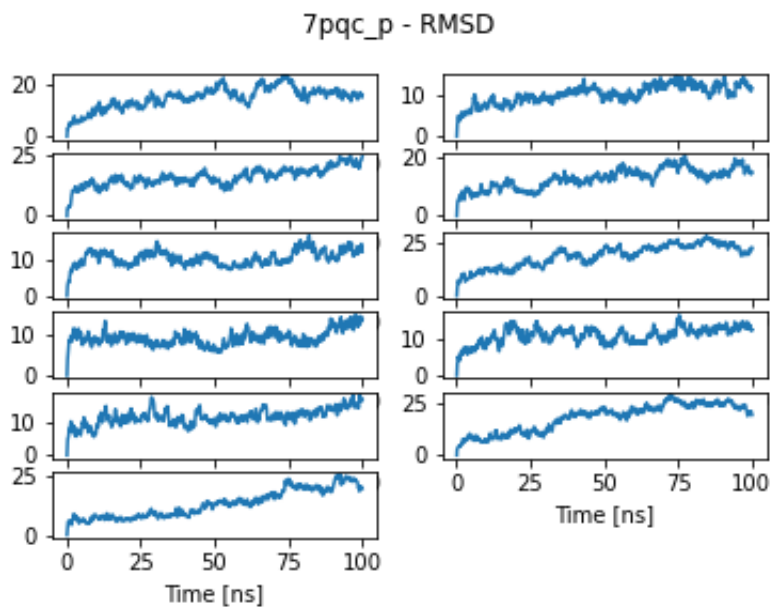


Figure 3.17: RMSD values, 11 simulations of 100ns, 7pqc phosphorylated

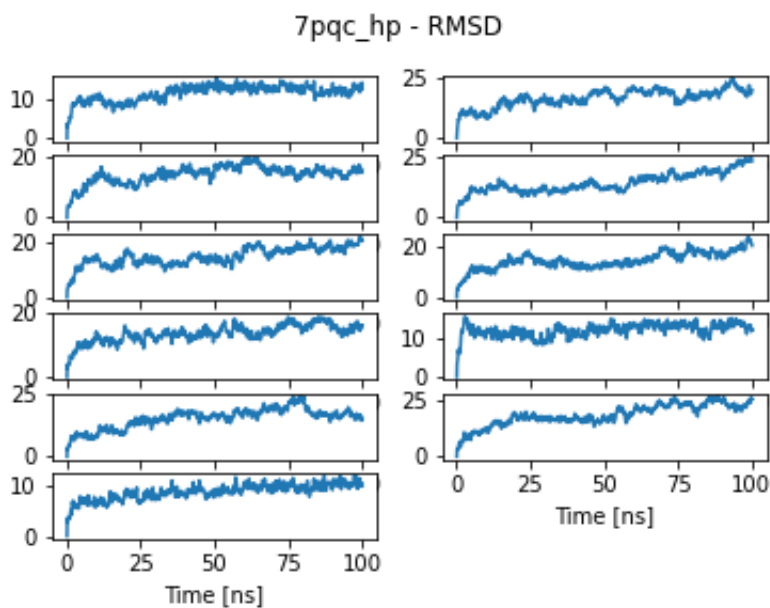


Figure 3.18: RMSD values, 11 simulations of 100ns, 7pqc human - phosphorylated

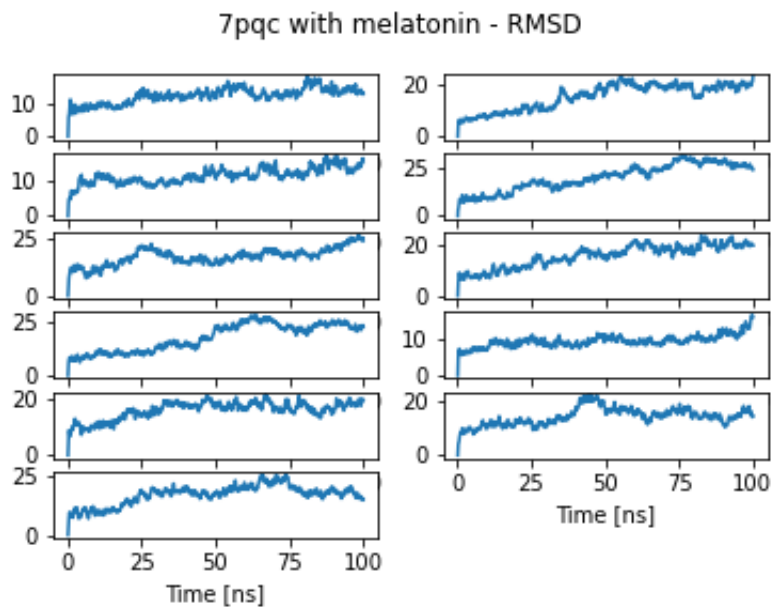


Figure 3.19: RMSD values, 11 simulations of 100ns, 7pqc with melatonin

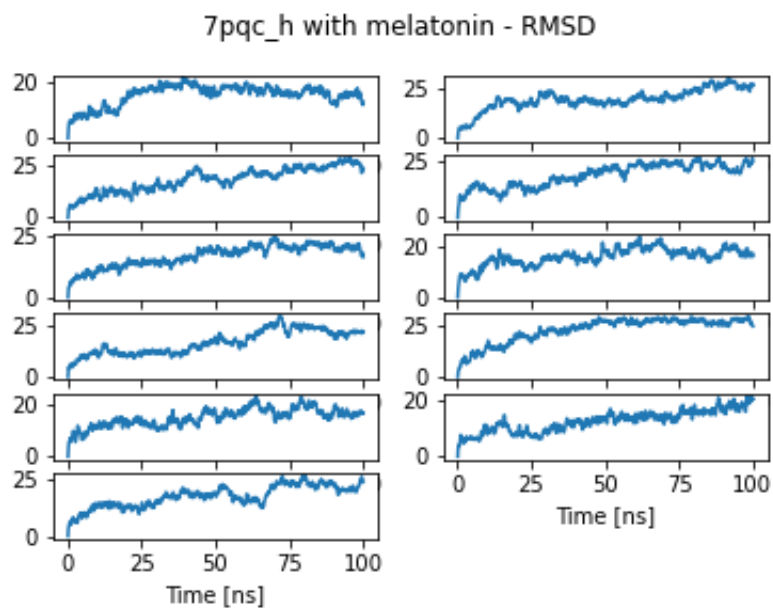


Figure 3.20: RMSD values, 11 simulations of 100ns, 7pqc human with melatonin

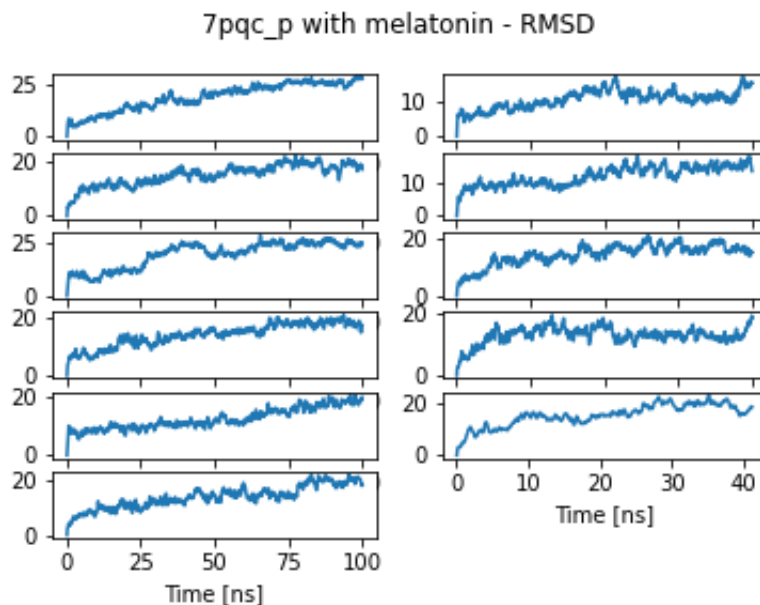


Figure 3.21: RMSD values, 11 simulations of 100ns, 7pqc phosphorylated with melatonin

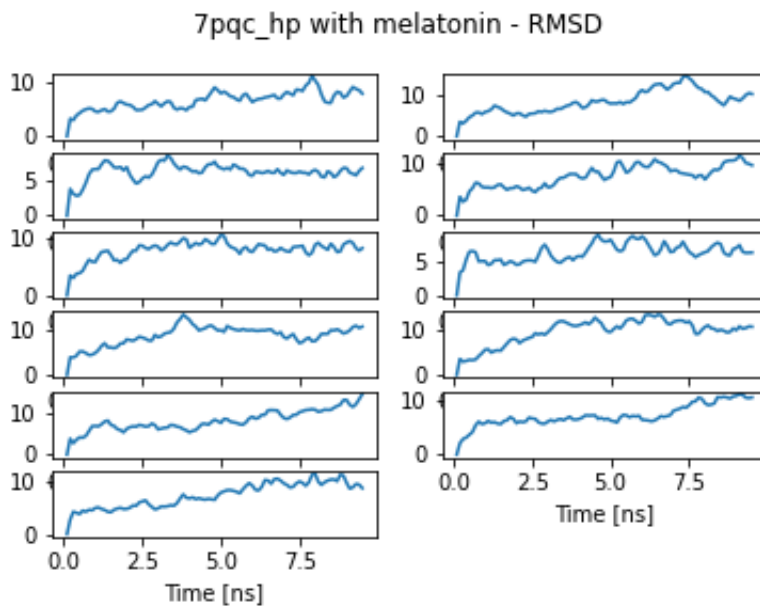


Figure 3.22: RMSD values, 11 simulations of 100ns, 7pqc human-phosphorylated with melatonin

3.4 Free-binding energy estimation

In total, 8 structures have been constructed and the free-binding energy of tau to microtubules was calculated. In addition, it has been estimated the contribution of each serine.

7pqc	7pqc_h	7pqc_p	7pqc_hp
-197.7 ± 44	-202.2 ± 46	116.1 ± 68	79.9 ± 54

Table 3.19: Free-binding energy [kJ/mol], Tau-Microtubules, No-melatonin

7pqc	7pqc_h	7pqc_p	7pqc_hp
-175.1 ± 57.6	-183.1 ± 44.4	204.6 ± 50.6	86.3 ± 53.6

Table 3.20: Free-binding energy [kJ/mol], Tau-Microtubules with melatonin

	7pqc	7pqc_h	7pqc_p	7pqc_hp
SER208	-1.4 ± 3.6	-2.7 ± 2.8	1127.6 ± 121.3	1156 ± 124.2
SER210	-0.03 ± 2.1	0.69 ± 4	1126.2 ± 114.7	1167 ± 125.5
SER214	-1.9 ± 1.4	-3.3 ± 2.7	1140.3 ± 108.4	1174.9 ± 119.6
SER235	-1.1 ± 2.8	-4.1 ± 4	1262.8 ± 89.1	1205.7 ± 101.4
SER237	-3 ± 3.3	-2.6 ± 3.5	1311.4 ± 79.7	1238.8 ± 96
SER238	-2.1 ± 3.8	-1.6 ± 2.6	1311.6 ± 113.4	1235 ± 111.1
SER241	-3.9 ± 2.7	-3.4 ± 2.7	1287.4 ± 59.1	1214.4 ± 94.4
SER258	-6.3 ± 4.4	-10.2 ± 3.4	1328.4 ± 118.9	1202.7 ± 116.7
SER262	-6.2 ± 4.9	-7.6 ± 5.1	1288.6 ± 111.7	1139.6 ± 71.3
SER285	-2.8 ± 3	-5 ± 2.1	1321.4 ± 115.6	1251 ± 104.4
SER289	-12.7 ± 4.5	-12 ± 3.7	1302.4 ± 146.6	1114.5 ± 87.9
SER293	-5.3 ± 4.4	-3.5 ± 4.3	1273.7 ± 127.6	1101.8 ± 87.7
SER305	-2.2 ± 3.3	-3.5 ± 2.8	1218.8 ± 152.6	1121.7 ± 127.6
SER316	-0.4 ± 2.5	-1.9 ± 1.9	1109.3 ± 164.6	1098.9 ± 118.8
SER320	-9.9 ± 6.5	-4.7 ± 5.9	1085.3 ± 152	989.5 ± 142.1
SER324	-3.6 ± 5.8	-3.9 ± 3.8	1051.5 ± 147.5	962.8 ± 124.2
SER341	0.09 ± 0.5	0.002 ± 0.4	540.9 ± 21.9	521.4 ± 18.4
SER352	-0.4 ± 0.2	-0.4 ± 0.3	450.5 ± 11.8	432.5 ± 8.9
SER356	-0.7 ± 0.3	-0.8 ± 0.1	439.6 ± 11.6	421.6 ± 7.5

Table 3.21: Free-binding energy [kJ/mol], Tau-Microtubules with melatonin

3.4. FREE-BINDING ENERGY ESTIMATION

	7pqc	7pqc_h	7pqc_p	7pqc_hp
SER208	-1.1 ± 3	-1.9 ± 4	1191.3 ± 105.7	1124.8 ± 123.3
SER210	0.7 ± 1.5	-1.14 ± 3.3	1185.2 ± 102.1	1141.1 ± 120.2
SER214	-2.7 ± 2.4	-2.3 ± 1.5	1191.9 ± 106.5	1191.3 ± 131.5
SER235	-2.1 ± 3.3	-1.3 ± 2.1	1301.4 ± 92	1190.6 ± 105.4
SER237	-2.8 ± 3.4	-5 ± 3.6	1332.7 ± 121.7	1197.2 ± 113.2
SER238	-0.8 ± 4.9	-3.1 ± 3.1	1338.8 ± 109.1	1203.3 ± 105.3
SER241	-4.5 ± 1.8	-3.5 ± 3.1	1323.6 ± 136.3	1218.1 ± 146.7
SER258	-10.3 ± 3.9	-9.3 ± 4.1	1266.4 ± 109	1239.3 ± 91.7
SER262	-6.1 ± 5.5	-9.5 ± 7.2	1219.1 ± 82.9	1182.9 ± 103.2
SER285	-2.4 ± 4.6	-3.5 ± 2.7	1335 ± 165.3	1224.6 ± 122.6
SER289	-13.2 ± 2.9	-10.9 ± 4.1	1243 ± 191	1098.9 ± 97.7
SER293	-6.8 ± 6.6	-3.3 ± 1.7	1185.6 ± 162.9	1084.8 ± 92.1
SER305	-4 ± 4.3	-1 ± 2.1	1152 ± 173.6	1076.9 ± 119.9
SER316	-2 ± 3.2	-3.1 ± 2.9	1046.5 ± 169.7	1089.7 ± 148
SER320	-9.4 ± 6	-6 ± 7.7	909.6 ± 153.8	1010.8 ± 175.4
SER324	-5.1 ± 3.3	-3.7 ± 2.3	886.5 ± 129.5	987.1 ± 190.9
SER341	-0.18 ± 0.6	-0.08 ± 0.4	531.9 ± 44.6	536.6 ± 37.9
SER352	-0.5 ± 0.1	-0.3 ± 0.2	442.3 ± 18.8	436.8 ± 17.2
SER356	-0.7 ± 0.2	-0.5 ± 0.2	429.9 ± 17.2	424.9 ± 16.5

Table 3.22: Free-binding energy [kJ/mol], Tau-Microtubules, No-melatonin

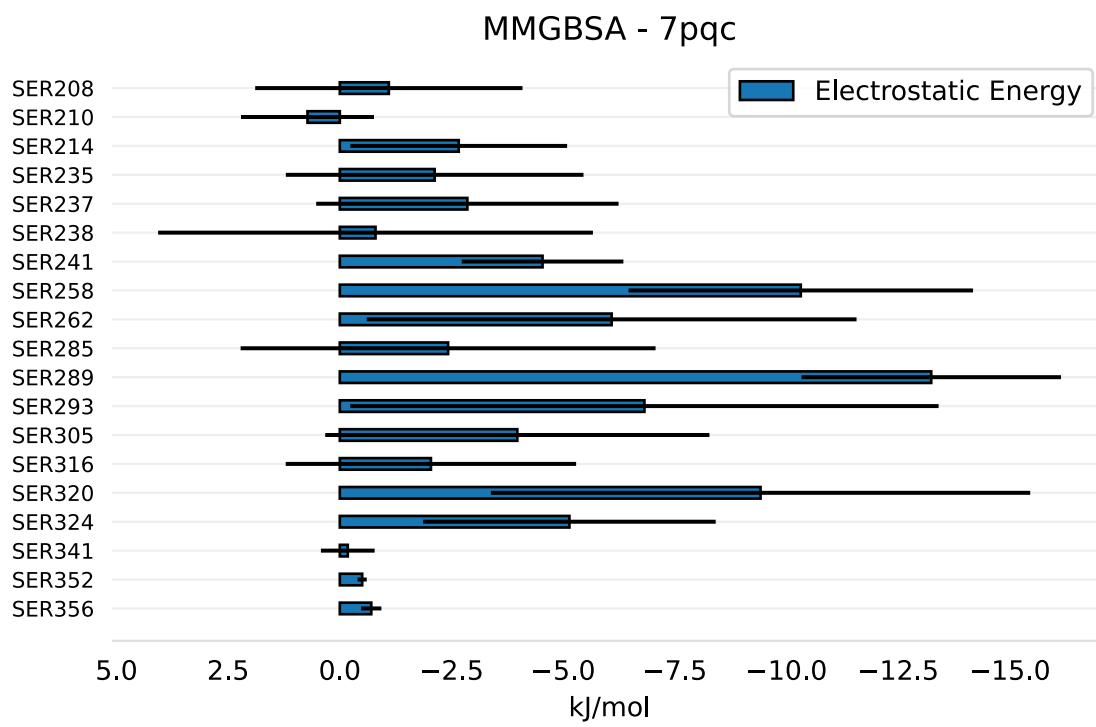


Figure 3.23: Free-binding energy of the binding of serines to microtubules. 7pqc

3.4. FREE-BINDING ENERGY ESTIMATION

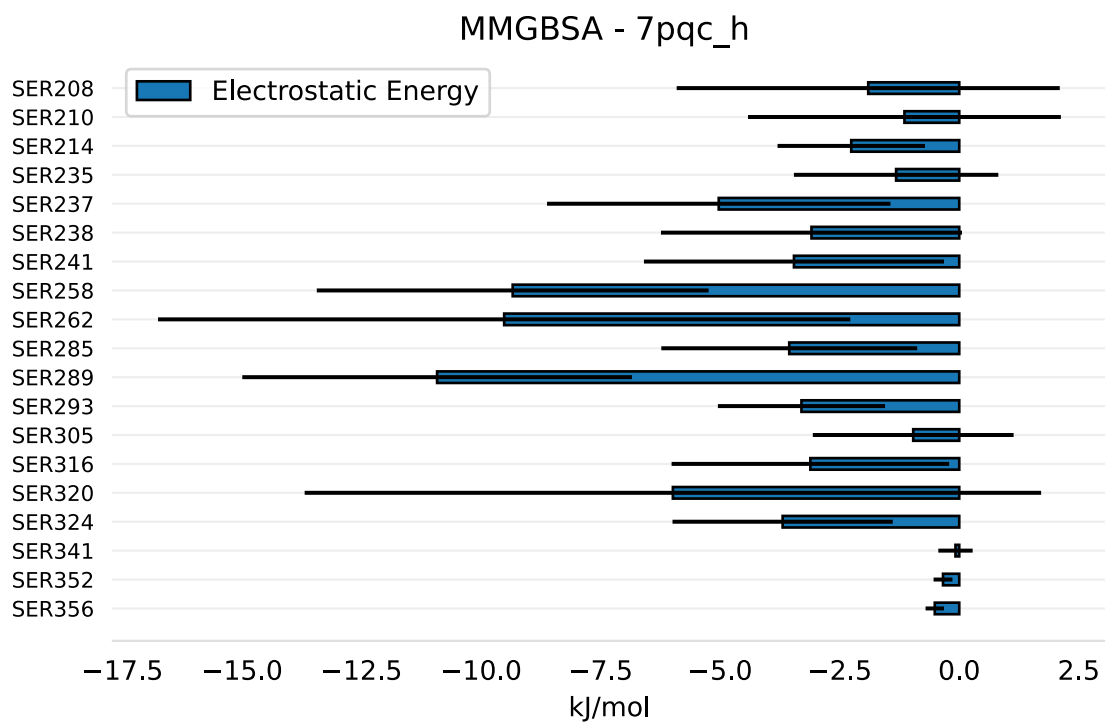


Figure 3.24: Free-binding energy of the binding of serines to microtubules. Human 7pqc

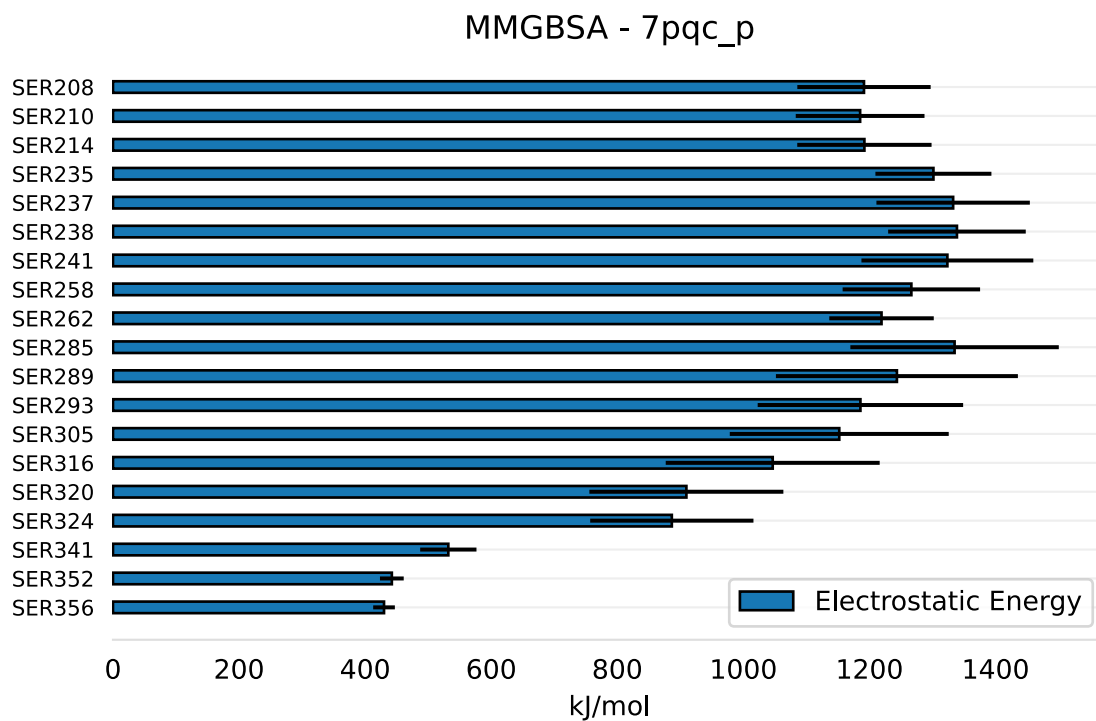


Figure 3.25: Free-binding energy of the binding of serines to microtubules. Phosphorylated 7pqc

3.4. FREE-BINDING ENERGY ESTIMATION

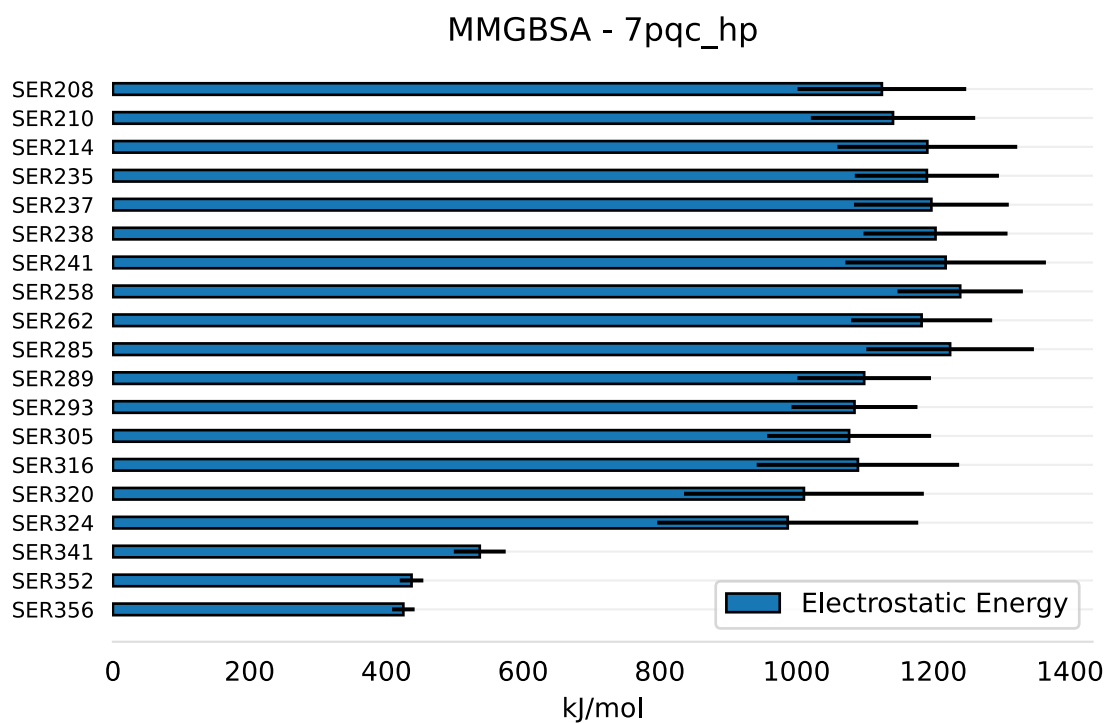


Figure 3.26: Free-binding energy of the binding of serines to microtubules. Human-phosphorylated 7pqc

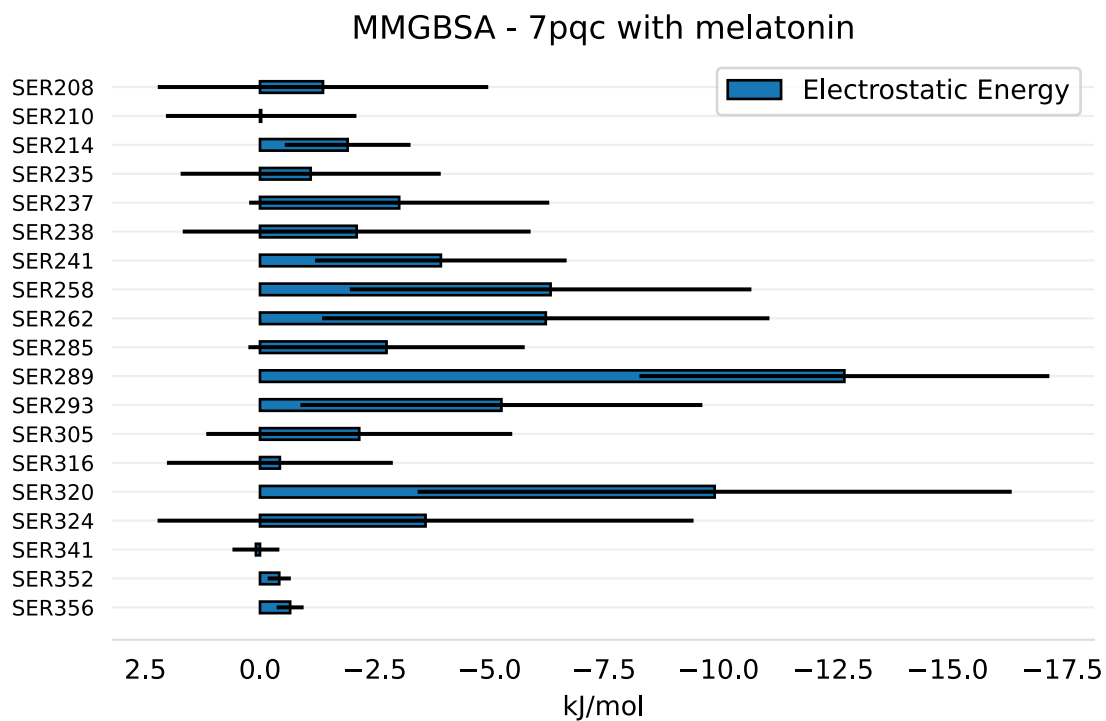


Figure 3.27: Free-binding energy of the binding of serines to microtubules. 7pqc with melatonin.

3.4. FREE-BINDING ENERGY ESTIMATION

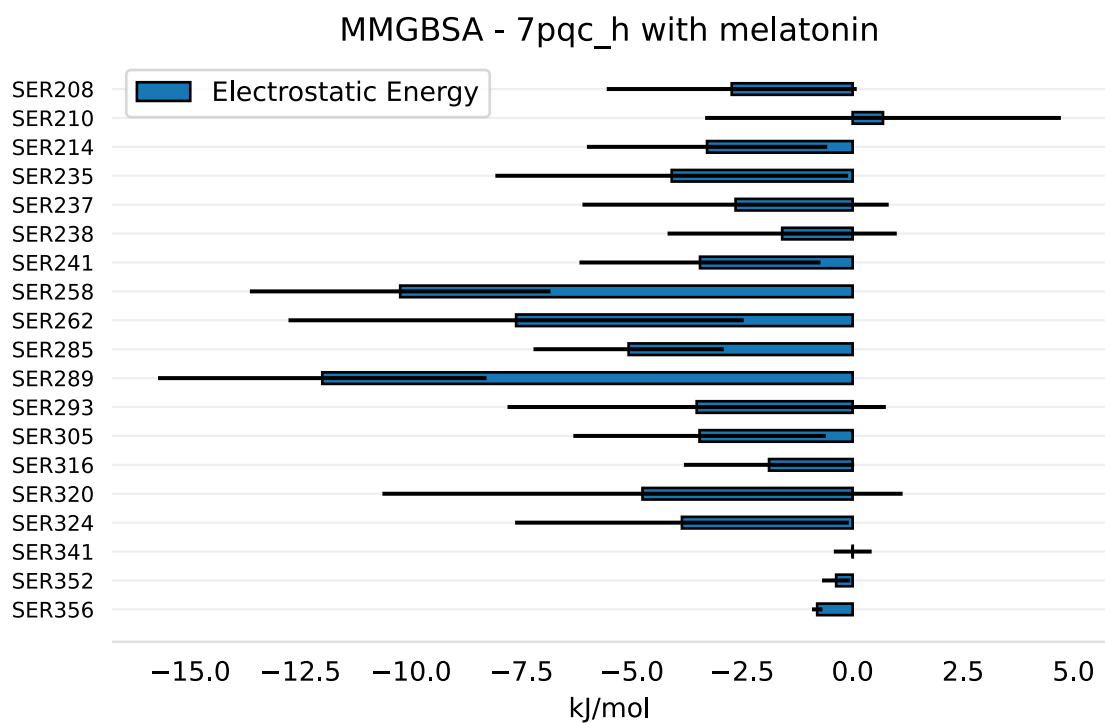


Figure 3.28: Free-binding energy of the binding of serines to microtubules. Human 7pqc with melatonin.

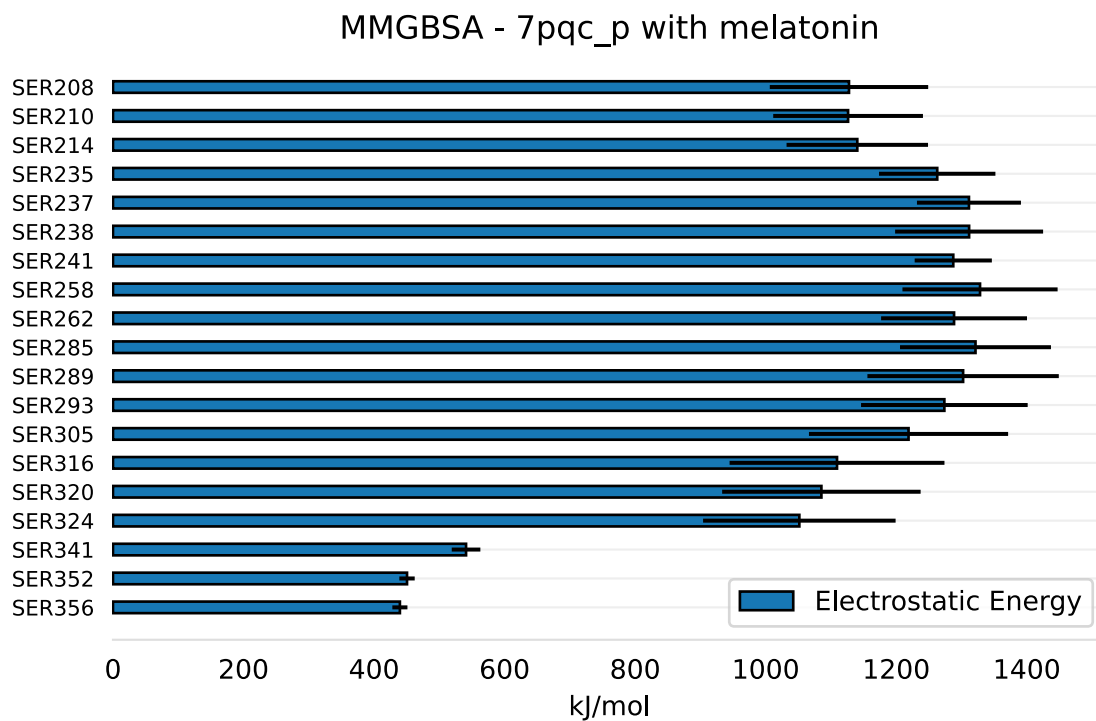


Figure 3.29: Free-binding energy of the binding of serines to microtubules. Phosphorylated 7pqc with melatonin.

3.4. FREE-BINDING ENERGY ESTIMATION

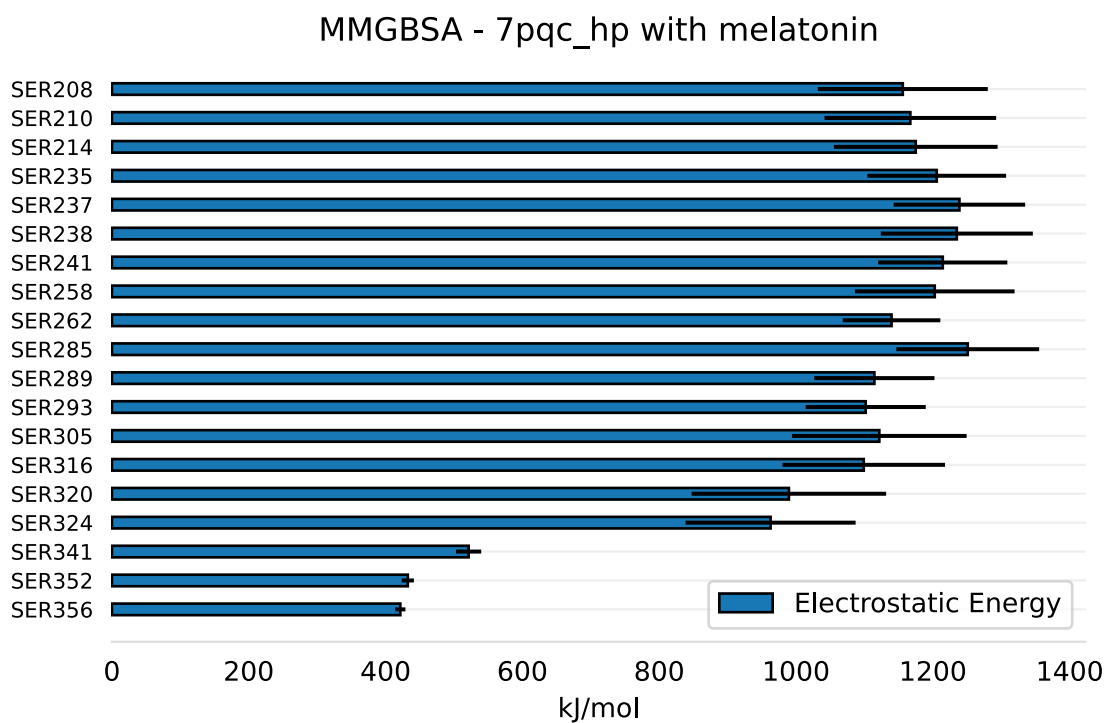


Figure 3.30: Free-binding energy of the binding of serines to microtubules. Human-phosphorylated 7pqc with melatonin.

Looking at the results, we can see the phosphorylation of serines strongly influences and, in particular, reduces the binding of tau to microtubules. However, this binding is not influenced by melatonin. Also, there is no difference between human and non-human structures.

4

Conclusions

Alzheimer's disease is the main neurodegenerative disease that currently afflicts our society. In this work, the effects of hyperphosphorylation of Tau have been investigated showing that this is the main factor that drives the detachment of Tau from microtubules. Unfortunately, the role of melatonin has not been well elucidated, opening questions that can be answered in further research. In particular, it is thought that melatonin can influence Tau phosphorylation by acting directly or indirectly on kinases and phosphatases such as GSK3 β , CaMKII and PP2A. Another factor that can be investigated is the role of Zinc in the progression of the disease. The main role of zinc is to help the assembling of microtubules so it is released in the intracellular environment after the disruption of microtubules and mediates the formation of neurofibrillary tangles. In addition, it can be a possible link between the disruption of microtubules and the formation of amyloid plaque in the extracellular environment. In fact, the release of Zinc in the extracellular environment could be the main factor that induces the nucleation of amyloid- β and the subsequent formation of amyloid plaques. All these phenomena could be driven by a change in the temperature and, in particular, by a lowered body temperature, which could explain why old people are more affected by Alzheimer's disease. So, this work is just an introduction to a bigger problem that currently is not well understood but that has seen an increased number of theories during the last years that tries to explain it. In particular, the Temperature theory could be

the one that could explain why Alzheimer's disease seems to be driven by several factors at the same time.

Bibliography

- [1] D. Wang, X. Huang, L. Yan, L. Zhou, C. Yan, J. Wu, Z. Su, and Y. Huang, "The structure biology of tau and clue for aggregation inhibitor design," *The Protein Journal*, vol. 40, pp. 656–668, Aug. 2021.
- [2] T. J. Dolinsky, J. E. Nielsen, J. A. McCammon, and N. A. Baker, "PDB2pqr: an automated pipeline for the setup of poisson-boltzmann electrostatics calculations," *Nucleic Acids Research*, vol. 32, pp. W665–W667, July 2004.
- [3] "Alzheimer's disease facts and figures, 2022." <https://www.alz.org/alzheimers-dementia/facts-figures>.
- [4] U. Kishore, ed., *Neurodegenerative Diseases*. InTech, May 2013.
- [5] A. Delacourte and A. Defossez, "Alzheimer's disease: Tau proteins, the promoting factors of microtubule assembly, are major components of paired helical filaments," *Journal of the Neurological Sciences*, vol. 76, pp. 173–186, Dec. 1986.
- [6] E. Karran, M. Mercken, and B. D. Strooper, "The amyloid cascade hypothesis for alzheimer's disease: an appraisal for the development of therapeutics," *Nature Reviews Drug Discovery*, vol. 10, pp. 698–712, Aug. 2011.
- [7] S. I. A. Cohen, S. Linse, L. M. Luheshi, E. Hellstrand, D. A. White, L. Rajah, D. E. Otzen, M. Vendruscolo, C. M. Dobson, and T. P. J. Knowles, "Proliferation of amyloid- β 42 aggregates occurs through a secondary nucleation mechanism," *Proceedings of the National Academy of Sciences*, vol. 110, no. 24, pp. 9758–9763, 2013.
- [8] C. Piller, "Potential fabrication in research images threatens key theory of alzheimer's disease," Jul 2022.

- [9] I. Grundke-Iqbal, K. Iqbal, Y. C. Tung, M. Quinlan, H. M. Wisniewski, and L. I. Binder, "Abnormal phosphorylation of the microtubule-associated protein tau (tau) in alzheimer cytoskeletal pathology.," *Proceedings of the National Academy of Sciences*, vol. 83, no. 13, pp. 4913–4917, 1986.
- [10] Y. IHARA, N. NUKINA, R. MIURA, and M. OGAWARA, "Phosphorylated tau protein is integrated into paired helical filaments in alzheimer's disease," *The Journal of Biochemistry*, vol. 99, no. 6, pp. 1807–1810, 1986.
- [11] M. D. Weingarten, A. H. Lockwood, S. Y. Hwo, and M. W. Kirschner, "A protein factor essential for microtubule assembly.," *Proceedings of the National Academy of Sciences*, vol. 72, no. 5, pp. 1858–1862, 1975.
- [12] M. Goedert, M. G. Spillantini, M. C. Potier, J. Ulrich, and R. A. Crowther, "Cloning and sequencing of the cDNA encoding an isoform of microtubule-associated protein tau containing four tandem repeats: differential expression of tau protein mRNAs in human brain.," *The EMBO Journal*, vol. 8, no. 2, pp. 393–399, 1989.
- [13] A. Himmler, D. Drechsel, M. W. Kirschner, and D. W. Martin, "Tau consists of a set of proteins with repeated c-terminal microtubule-binding domains and variable n-terminal domains," *Molecular and Cellular Biology*, vol. 9, no. 4, pp. 1381–1388, 1989.
- [14] M. D. Mukrasch, S. Bibow, J. Korukottu, S. Jeganathan, J. Biernat, C. Griesinger, E. Mandelkow, and M. Zweckstetter, "Structural polymorphism of 441-residue tau at single residue resolution," *PLOS Biology*, vol. 7, pp. 1–1, 02 2009.
- [15] M. D. Mukrasch, P. Markwick, J. Biernat, M. von Bergen, P. Bernadó, C. Griesinger, E. Mandelkow, M. Zweckstetter, and M. Blackledge, "Highly populated turn conformations in natively unfolded tau protein identified from residual dipolar couplings and molecular simulation," *Journal of the American Chemical Society*, vol. 129, no. 16, pp. 5235–5243, 2007. PMID: 17385861.
- [16] M. Schwalbe, V. Ozenne, S. Bibow, M. Jaremko, L. Jaremko, M. Gajda, M. R. Jensen, J. Biernat, S. Becker, E. Mandelkow, M. Zweckstetter, and M. Blackledge, "Predictive Atomic Resolution Descriptions of Intrinsically Disordered hTau40 and α -Synuclein in Solution from NMR and Small Angle Scattering," *Structure*, vol. 22, no. 2, pp. 238–249, 2014.

- [17] M. von Bergen, P. Friedhoff, J. Biernat, J. Heberle, E.-M. Mandelkow, and E. Mandelkow, "Assembly of tau protein into alzheimer paired helical filaments depends on a local sequence motif (³⁰⁶VQIVYK³¹¹) forming β -structure," *Proceedings of the National Academy of Sciences*, vol. 97, no. 10, pp. 5129–5134, 2000.
- [18] E Köpke and Y.C. Tung and S Shaikh and A.C. Alonso and K Iqbal and I Grundke-Iqbal, "Microtubule-associated protein tau. abnormal phosphorylation of a non-paired helical filament pool in alzheimer disease.," *Journal of Biological Chemistry*, vol. 268, pp. 24374–24384, Nov. 1993.
- [19] E.-M. Mandelkow, G. Drewes, J. Biernat, N. Gustke, J. Van Lint, J. Vandenhede, and E. Mandelkow, "Glycogen synthase kinase-3 and the alzheimer-like state of microtubule-associated protein tau," *FEBS Letters*, vol. 314, no. 3, pp. 315–321, 1992.
- [20] J.-z. Wang, Q. Wu, A. Smith, I. Grundke-Iqbal, and K. Iqbal, " τ is phosphorylated by GSK-3 at several sites found in Alzheimer disease and its biological activity markedly inhibited only after it is prephosphorylated by A-kinase," *FEBS Letters*, vol. 436, no. 1, pp. 28–34, 1998.
- [21] J.-Z. Wang, I. Grundke-Iqbal, and K. Iqbal, "Kinases and phosphatases and tau sites involved in alzheimer neurofibrillary degeneration," *European Journal of Neuroscience*, vol. 25, no. 1, pp. 59–68, 2007.
- [22] J.-J. Pei, T. Tanaka, Y.-C. Tung, E. Braak, K. Iqbal, and I. Grundke-Iqbal, "Distribution, Levels, and Activity of Glycogen Synthase Kinase-3 in the Alzheimer Disease Brain," *Journal of Neuropathology Experimental Neurology*, vol. 56, pp. 70–78, 01 1997.
- [23] Q. Zheng-Fischhöfer, J. Biernat, E.-M. Mandelkow, S. Illenberger, R. Gode mann, and E. Mandelkow, "Sequential phosphorylation of tau by glycogen synthase kinase-3 and protein kinase a at thr212 and ser214 generates the alzheimer-specific epitope of antibody at100 and requires a paired-helical-filament-like conformation," *European Journal of Biochemistry*, vol. 252, no. 3, pp. 542–552, 1998.
- [24] T. J. Singh, T. Zaidi, I. Grundke-Iqbal, and K. Iqbal, "Modulation of gsk-3-catalyzed phosphorylation of microtubule-associated protein tau by non-proline-dependent protein kinases," *FEBS Letters*, vol. 358, no. 1, pp. 4–8, 1995.

- [25] C. A. Rankin, Q. Sun, and T. C. Gamblin, "Tau phosphorylation by GSK-3 promotes tangle-like filament morphology," *Molecular Neurodegeneration*, vol. 2, June 2007.
- [26] J. Rowles, C. Slaughter, C. Moomaw, J. Hsu, and M. H. Cobb, "Purification of casein kinase i and isolation of cDNAs encoding multiple casein kinase i-like enzymes.," *Proceedings of the National Academy of Sciences*, vol. 88, pp. 9548–9552, Nov. 1991.
- [27] S. D. Gross and R. A. Anderson, "Casein kinase i," *Cellular Signalling*, vol. 10, pp. 699–711, Nov. 1998.
- [28] K. Yasojima, J. Kuret, A. J. DeMaggio, E. McGeer, and P. L. McGeer, "Casein kinase 1 delta mRNA is upregulated in alzheimer disease brain," *Brain Research*, vol. 865, pp. 116–120, May 2000.
- [29] G. Li, H. Yin, and J. Kuret, "Casein kinase 1 delta phosphorylates tau and disrupts its binding to microtubules," *Journal of Biological Chemistry*, vol. 279, pp. 15938–15945, Apr. 2004.
- [30] D. P. Hanger, H. L. Byers, S. Wray, K.-Y. Leung, M. J. Saxton, A. Seereeram, C. H. Reynolds, M. A. Ward, and B. H. Anderton, "Novel phosphorylation sites in tau from alzheimer brain support a role for casein kinase 1 in disease pathogenesis," *Journal of Biological Chemistry*, vol. 282, pp. 23645–23654, Aug. 2007.
- [31] J. B. Myers, V. Zaegel, S. J. Coultrap, A. P. Miller, K. U. Bayer, and S. L. Reichow, "The CaMKII holoenzyme structure in activation-competent conformations," *Nature Communications*, vol. 8, June 2017.
- [32] J. Lisman, R. Yasuda, and S. Raghavachari, "Mechanisms of CaMKII action in long-term potentiation," *Nature Reviews Neuroscience*, vol. 13, pp. 169–182, Feb. 2012.
- [33] T. J. A. Craddock, J. A. Tuszynski, and S. Hameroff, "Cytoskeletal signaling: Is memory encoded in microtubule lattices by CaMKII phosphorylation?," *PLoS Computational Biology*, vol. 8, pp. 1–16, Mar. 2012.
- [34] J. Biernat, N. Gustke, G. Drewes, E.-. Mandelkow, and E. Mandelkow, "Phosphorylation of ser262 strongly reduces binding of tau to microtubules: Distinction between PHF-like immunoreactivity and microtubule binding," *Neuron*, vol. 11, pp. 153–163, July 1993.

- [35] T. J. Singh, J.-Z. Wang, M. Novak, E. Kontzekova, I. Grundke-Iqbal, and K. Iqbal, "Calcium/calmodulin-dependent protein kinase II phosphorylates tau at ser-262 but only partially inhibits its binding to microtubules," *FEBS Letters*, vol. 387, pp. 145–148, June 1996.
- [36] J. J. Sironi, S.-H. Yen, J. A. Gondal, Q. Wu, I. Grundke-Iqbal, and K. Iqbal, "Ser-262 in human recombinant tau protein is a markedly more favorable site for phosphorylation by CaMKII than PKA or PhK," *FEBS Letters*, vol. 436, pp. 471–475, Oct. 1998.
- [37] A. Schneider, J. Biernat, M. von Bergen, E. Mandelkow, and E.-M. Mandelkow, "Phosphorylation that detaches tau protein from microtubules (ser262, ser214) also protects it against aggregation into alzheimer paired helical filaments," *Biochemistry*, vol. 38, pp. 3549–3558, Mar. 1999.
- [38] M. Necula and J. Kuret, "Pseudophosphorylation and glycation of tau protein enhance but do not trigger fibrillization in vitro," *Journal of Biological Chemistry*, vol. 279, pp. 49694–49703, Nov. 2004.
- [39] Y. Huang, Z. Wu, Y. Cao, M. Lang, B. Lu, and B. Zhou, "Zinc binding directly regulates tau toxicity independent of tau hyperphosphorylation," *Cell Reports*, vol. 8, pp. 831–842, Aug. 2014.
- [40] F. Liu, I. Grundke-Iqbal, K. Iqbal, and C.-X. Gong, "Contributions of protein phosphatases PP1, PP2A, PP2B and PP5 to the regulation of tau phosphorylation," *European Journal of Neuroscience*, vol. 22, pp. 1942–1950, Oct. 2005.
- [41] C.-X. Gong, T. J. Singh, I. Grundke-Iqbal, and K. Iqbal, "Phosphoprotein phosphatase activities in alzheimer disease brain," *Journal of Neurochemistry*, vol. 61, pp. 921–927, Sept. 1993.
- [42] C.-X. Gong, S. Shaikh, J.-Z. Wang, T. Zaidi, I. Grundke-Iqbal, and K. Iqbal, "Phosphatase activity toward abnormally phosphorylated : Decrease in alzheimer disease brain," *Journal of Neurochemistry*, vol. 65, pp. 732–738, Nov. 2002.
- [43] H. Tanimukai, I. Grundke-Iqbal, and K. Iqbal, "Up-Regulation of Inhibitors of Protein Phosphatase-2A in Alzheimer's Disease," *The American Journal of Pathology*, vol. 166, pp. 1761–1771, June 2005.

- [44] L. Arnaud, S. Chen, F. Liu, B. Li, S. Khatoon, I. Grundke-Iqbal, and K. Iqbal, "Mechanism of inhibition of PP2A activity and abnormal hyperphosphorylation of tau by I_1^{PP2A}/SET ," *FEBS Letters*, vol. 585, pp. 2653–2659, July 2011.
- [45] G. Basurto-Islas, I. Grundke-Iqbal, Y. C. Tung, F. Liu, and K. Iqbal, "Activation of Asparaginyl Endopeptidase Leads to Tau Hyperphosphorylation in Alzheimer Disease," *Journal of Biological Chemistry*, vol. 288, pp. 17495–17507, June 2013.
- [46] V. Theendakara, D. E. Bredesen, and R. V. Rao, "Downregulation of protein phosphatase 2A by apolipoprotein E: Implications for Alzheimer's disease," *Molecular and Cellular Neuroscience*, vol. 83, pp. 83–91, Sept. 2017.
- [47] M. Bennecib, C.-X. Gong, I. Grundke-Iqbal, and K. Iqbal, "Inhibition of PP-2a upregulates CaMKII in rat forebrain and induces hyperphosphorylation of tau at ser 262/356," *FEBS Letters*, vol. 490, pp. 15–22, Feb. 2001.
- [48] W. Qian, J. Shi, X. Yin, K. Iqbal, I. Grundke-Iqbal, C.-X. Gong, and F. Liu, "PP2a regulates tau phosphorylation directly and also indirectly via activating GSK-3," *Journal of Alzheimer's Disease*, vol. 19, pp. 1221–1229, Mar. 2010.
- [49] E. Planel, "Alterations in glucose metabolism induce hypothermia leading to tau hyperphosphorylation through differential inhibition of kinase and phosphatase activities: Implications for alzheimer's disease," *Journal of Neuroscience*, vol. 24, pp. 2401–2411, Mar. 2004.
- [50] E. Planel, A. Bretteville, L. Liu, L. Virag, A. L. Du, W. H. Yu, D. W. Dickson, R. A. Whittington, and K. E. Duff, "Acceleration and persistence of neurofibrillary pathology in a mouse model of tauopathy following anesthesia," *The FASEB Journal*, vol. 23, pp. 2595–2604, Mar. 2009.
- [51] M. Tournissac, M. Leclerc, J. Valentin-Escalera, M. Vandal, C. R. Bosoi, E. Planel, and F. Calon, "Metabolic determinants of alzheimer's disease: A focus on thermoregulation," *Ageing Research Reviews*, vol. 72, p. 101462, Dec. 2021.
- [52] I. Guisle, M. Gratuze, S. Petry, F. Morin, R. Keraudren, R. A. Whittington, S. S. Hébert, V. Mongrain, and E. Planel, "Circadian and sleep/wake-dependent variations in tau phosphorylation are driven by temperature," *Sleep*, vol. 43, Nov. 2019.

- [53] E. Planel, K. E. G. Richter, C. E. Nolan, J. E. Finley, L. Liu, Y. Wen, P. Krishnamurthy, M. Herman, L. Wang, J. B. Schachter, R. B. Nelson, L.-F. Lau, and K. E. Duff, "Anesthesia leads to tau hyperphosphorylation through inhibition of phosphatase activity by hypothermia," *Journal of Neuroscience*, vol. 27, pp. 3090–3097, Mar. 2007.
- [54] P. N. Tariot, "Chronic divalproex sodium to attenuate agitation and clinical progression of alzheimer disease," *Archives of General Psychiatry*, vol. 68, p. 853, Aug. 2011.
- [55] O. V. Forlenza, V. J. R. De-Paula, and B. S. O. Diniz, "Neuroprotective effects of lithium: Implications for the treatment of alzheimer's disease and related neurodegenerative disorders," *ACS Chemical Neuroscience*, vol. 5, pp. 443–450, May 2014.
- [56] S. Lovestone, M. Boada, B. Dubois, M. Hüll, J. O. Rinne, H.-J. Huppertz, M. Calero, M. V. Andrés, B. Gómez-Carrillo, T. León, and T. del Ser and, "A phase II trial of tideglusib in alzheimer's disease," *Journal of Alzheimer's Disease*, vol. 45, pp. 75–88, Mar. 2015.
- [57] J. Hui, J. Zhang, M. Pu, X. Zhou, L. Dong, X. Mao, G. Shi, J. Zou, J. Wu, D. Jiang, and G. Xi, "Modulation of GSK-3 β β -Catenin signaling contributes to learning and memory impairment in a rat model of depression," *International Journal of Neuropsychopharmacology*, vol. 21, pp. 858–870, Apr. 2018.
- [58] T. Kramer, B. Schmidt, and F. L. Monte, "Small-molecule inhibitors of GSK-3: Structural insights and their application to alzheimer's disease models," *International Journal of Alzheimer's Disease*, vol. 2012, pp. 1–32, 2012.
- [59] R. Bhat, Y. Xue, S. Berg, S. Hellberg, M. Ormö, Y. Nilsson, A.-C. Radesäter, E. Jerning, P.-O. Markgren, T. Borgegård, M. Nylöf, A. Giménez-Cassina, F. Hernández, J. J. Lucas, J. Díaz-Nido, and J. Avila, "Structural insights and biological effects of glycogen synthase kinase 3-specific inhibitor AR-a014418," *Journal of Biological Chemistry*, vol. 278, pp. 45937–45945, Nov. 2003.
- [60] M. Leost, C. Schultz, A. Link, Y.-Z. Wu, J. Biernat, E.-M. Mandelkow, J. A. Bibb, G. L. Snyder, P. Greengard, D. W. Zaharevitz, R. Gussio, A. M. Senderowicz, E. A. Sausville, C. Kunick, and L. Meijer, "Paullones are potent inhibitors of glycogen synthase kinase-3 and cyclin-dependent kinase 5/p25," *European Journal of Biochemistry*, vol. 267, pp. 5983–5994, Oct. 2000.

- [61] A. D. Simone, V. Tumiatti, V. Andrisano, and A. Milelli, "Glycogen Synthase Kinase 3 β : A New Gold Rush in Anti-Alzheimer's Disease Multitarget Drug Discovery?," *Journal of Medicinal Chemistry*, vol. 64, pp. 26–41, Dec. 2020.
- [62] C.-X. Gong, C.-L. Dai, F. Liu, and K. Iqbal, "Multi-Targets: An Unconventional Drug Development Strategy for Alzheimer's Disease," *Frontiers in Aging Neuroscience*, vol. 14, Feb. 2022.
- [63] F. Prati, A. De Simone, P. Bisignano, A. Armirotti, M. Summa, D. Pizzirani, R. Scarpelli, D. I. Perez, V. Andrisano, A. Perez-Castillo, B. Monti, F. Massenzio, L. Polito, M. Racchi, A. D. Favia, G. Bottegoni, A. Martinez, M. L. Bolognesi, and A. Cavalli, "Multitarget drug discovery for alzheimer's disease: Triazinones as BACE-1 and GSK-3 β inhibitors," *Angewandte Chemie International Edition*, vol. 54, pp. 1578–1582, Dec. 2014.
- [64] M. Yanagisawa, E. Planel, K. Ishiguro, and S. C. Fujita, "Starvation induces tau hyperphosphorylation in mouse brain: implications for alzheimer's disease," *FEBS Letters*, vol. 461, pp. 329–333, Nov. 1999.
- [65] T. Arendt, J. Stieler, A. M. Strijkstra, R. A. Hut, J. Rüdiger, E. A. V. der Zee, T. Harkany, M. Holzer, and W. Härtig, "Reversible paired helical filament-like phosphorylation of tau is an adaptive process associated with neuronal plasticity in hibernating animals," *The Journal of Neuroscience*, vol. 23, pp. 6972–6981, Aug. 2003.
- [66] R. A. Whittington, M.-A. Papon, F. Chouinard-Decorte, and E. Planel, "Hypothermia and alzheimers disease neuropathogenic pathways," *Current Alzheimer Research*, vol. 7, pp. 717–725, Dec. 2010.
- [67] J. T. Stieler, T. Bullmann, F. Kohl, Ø. Tøien, M. K. Brückner, W. Härtig, B. M. Barnes, and T. Arendt, "The physiological link between metabolic rate depression and tau phosphorylation in mammalian hibernation," *PLoS ONE*, vol. 6, p. e14530, Jan. 2011.
- [68] Y. Wang, Y. Zhang, W. Hu, S. Xie, C.-X. Gong, K. Iqbal, and F. Liu, "Rapid alteration of protein phosphorylation during postmortem: implication in the study of protein phosphorylation," *Scientific Reports*, vol. 5, Oct. 2015.
- [69] M. Gratuze, N. B. E. Khoury, A. Turgeon, C. Julien, F. Marcouiller, F. Morin, R. A. Whittington, A. Murette, F. Calon, and E. Planel, "Tau hyperphosphorylation in the brain of ob/ob mice is due to hypothermia: Importance of

- thermoregulation in linking diabetes and alzheimer's disease," *Neurobiology of Disease*, vol. 98, pp. 1–8, Feb. 2017.
- [70] M. Tournissac, P. Bourassa, R. D. Martinez-Cano, T.-M. Vu, S. S. Hébert, E. Planel, and F. Calon, "Repeated cold exposures protect a mouse model of alzheimer's disease against cold-induced tau phosphorylation," *Molecular Metabolism*, vol. 22, pp. 110–120, Apr. 2019.
- [71] E. M. Blessing, A. Parekh, R. A. Betensky, J. Babb, N. Saba, L. Debure, A. W. Varga, I. Ayappa, D. M. Rapoport, T. A. Butler, M. J. de Leon, T. Wisniewski, B. J. Lopresti, and R. S. Osorio, "Association between lower body temperature and increased tau pathology in cognitively normal older adults," *Neurobiology of Disease*, vol. 171, p. 105748, Sept. 2022.
- [72] E. Jurrus, D. Engel, K. Star, K. Monson, J. Brandi, L. E. Felberg, D. H. Brookes, L. Wilson, J. Chen, K. Liles, M. Chun, P. Li, D. W. Gohara, T. Dolinsky, R. Konecny, D. R. Koes, J. E. Nielsen, T. Head-Gordon, W. Geng, R. Krasny, G.-W. Wei, M. J. Holst, J. A. McCammon, and N. A. Baker, "Improvements to the scpAPBS/scp biomolecular solvation software suite," *Protein Science*, vol. 27, pp. 112–128, Oct. 2017.
- [73] S. Unni, Y. Huang, R. M. Hanson, M. Tobias, S. Krishnan, W. W. Li, J. E. Nielsen, and N. A. Baker, "Web servers and services for electrostatics calculations with APBS and PDB2pqr," *Journal of Computational Chemistry*, vol. 32, pp. 1488–1491, Feb. 2011.